Design and Specification of an Attitude Control System for the DANDE Mission

by

Brady W. Young

S.B., Massachusetts Institute of Technology, 2006

A thesis submitted to the

Faculty of the Graduate School of the

University of Colorado in partial fulfillment

of the requirements for the degree of

Master of Science

Department of Aerospace Engineering Sciences

2008

This thesis entitled:
Design and Specification of an Attitude Control System for the DANDE Mission
written by Brady W. Young
has been approved for the Department of Aerospace Engineering Sciences

Hanspeter Schaub

Assistant Professor Scott E. Palo

Date

The final copy of this thesis has been examined by the signatories, and we find that both the content and the form meet acceptable presentation standards of scholarly work in the above mentioned discipline.

Young, Brady W. (M.S., Aerospace Engineering Sciences)

Design and Specification of an Attitude Control System for the DANDE Mission

Thesis directed by Associate Professor, H. Joseph Smead Fellow Hanspeter Schaub

This thesis documents the design of an Attitude Determination and Control (ADC) subsystem for a 50 kg, low Earth orbiting space weather probe. The work emphasizes three major tasks: an architecture trade study, an analysis of the spinup maneuver, and a demonstration of the attitude determination method.

This document follows the systems engineering process used to design the ADC subsystem in the context of the Drag and Atmospheric Neutral Density Explorer (DANDE) mission. A number of missions relevant to the design of the DANDE spacecraft are reviewed. Some missions are similar to DANDE in their design constraints (e.g., student satellites), others serve as examples of successfully implemented design decisions.

A subsystem architecture trade study is then performed, leading to the key design decisions in the ADC subsystem: DANDE is a major-axis spinning spacecraft, spinning at 10 RMP about the orbit normal vector. DANDE attains its required spin rate in a closed loop algorithm and is aligned open loop. DANDE determines partial attitude using a magnetometer during spinup, then full spin axis determination is accomplished using Horizon Crossing Indicators. Active control is performed using magnetic torque rods, and nutation is passively damped with a fluid-filled ring.

Lower level requirements are then derived from the subsystem level requirements, and each actuator is designed according to these requirements.

An attitude simulation program is designed and implemented in MATLAB. This model is used to perform an analysis of the spinup maneuver, demonstrating that the subsystem is capable of spinning up the spacecraft from an unknown initial state within the time required. A baseline algorithm is tested, then refined to mitigate conditions

that could prevent spinup from completing within the budgeted time.

To validate requirements on the attitude determination hardware, a spin axis determination scheme is presented, and a worst-case analysis performed. The study generates a reference attitude profile in software, models the sensor response to the environment, and calculates the determined attitude. This is compared against the reference attitude and used to find the minimum quantity of sensor data needed to meet the attitude determination requirements.

Dedication

This work is dedicated to the student members of the DANDE team. Your accomplishments and your energy have been nothing less than inspirational.

Acknowledgements

I would like to thank the following individuals for their support on this work:

Dr. Hanspeter Schaub, my adviser, for keeping me on time and on track, and for his help on a wide range of technical issues.

Dr. Scott Palo and Dr. Dale Lawrence, for reading this work and sitting on my committee.

Dr. Tim Holden, my industry mentor, for first sparking my interest in attitude control and providing a well of information on the SNOE mission.

Chris Koehler, Director of the Colorado Space Grant Consortium, who not only funded my work on DANDE, but was instrumental in helping me find a job after graduation.

Marcin Pilinski, DANDE's Project Manager, whos tremendous technical breadth is only outdone only by his exceptional good nature.

Lucas Ward, my co-lead on DANDE's Attitude team for the first five months of the project.

Bradley Brisnehan, for his contributions to the design and manufacture of the torque rods and nutation damper.

Karina Ogilvie, for taking superb care of DANDE's mass properties.

Mike Grusin, Bruce Davis, Diana Loucks, Markus Wilde, Emily Walters, Brandon Gilles, James Gorman, Eric Dickey, Andrew Tomchek, Casey Kuhns and the rest of the DANDE team, who made going to work every day a pleasure.

Contents

Chapter

Tables

Table

Figures

Figure

Chapter 1

Introduction

Over the course of 15 months, an Attitude Determination and Control (ADC) subsystem was developed for a student microsatellite. This thesis documents the progression of the design from inception to the Critical Design Review (CDR) level.

The scope of this thesis includes three major areas of work:

(1) Designing the attitude subsystem architecture and selecting a the appropriate suite of hardware

(2) Analysis of a maneuver to bring the spacecraft from an unknown initial tumble to the nominal spin rate about the major principal axis

(3) Validation of the minimum quantity of attitude data required to meet the attitude determination requirements

Additionally, in order to perform the analysis necessary for the spinup maneuver, a spacecraft attitude simulation is also developed and documented in this text. This text does not include development of the control algorithm for aligning the spin axis of the spacecraft with the nominal orbit-normal direction. While this is a relevant and important portion of the DANDE mission, the open-loop control strategy allows this operation to be run from ground-element software. The focus of this thesis is the spacecraft hardware and baseline algorithm design, with the ground-element to be developed at a later date.

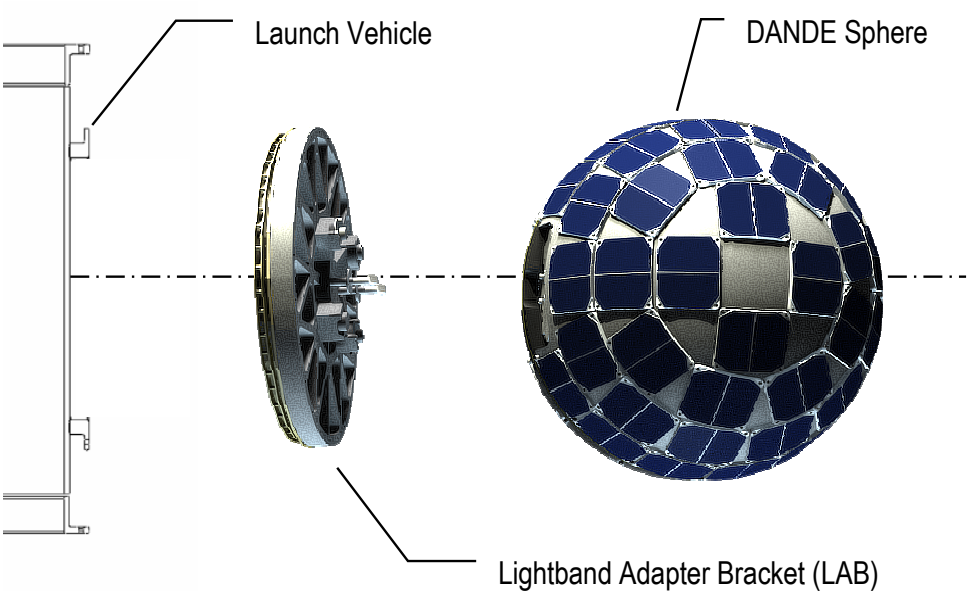

Figure 1.1: The DANDE space-sector components. Upon deployment, the launch vehicle ejects the LAB and sphere as a package. The sphere then separates from the LAB before the ADC system begins operation.

The Drag and Atmospheric Neutral Density Explorer (DANDE) spacecraft is a 50 kg, orbit-normal spinning probe designed to measure the atmospheric density and winds of the upper atmosphere between 150 and 350 km altitude. This is accomplished by combining data from an accelerometer payload (measuring the drag force on the spacecraft) and a mass spectrometer (measuring the frequency and energy of gas molecule impacts). The DANDE mission and high level requirements are discussed in greater detail in Chapter 3.

The science data requirements impose a number of uncommon challenges on the spacecraft subsystems. First, the data products are very sensitive to changes in the spacecraft coefficient of drag. To ensure the spacecraft has a uniform, well-characterized aerodynamic body, the DANDE spacecraft is built to be an 18" sphere. This uncommon volume constraint forces components to share a tighter space, heightening the problem

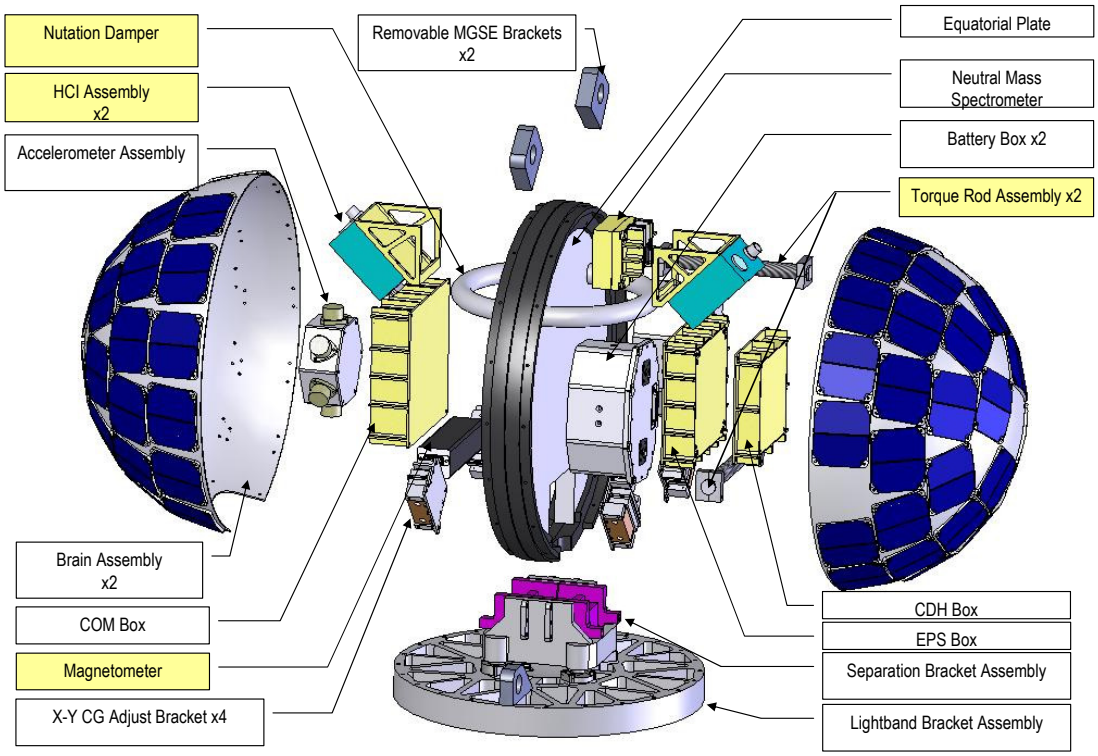

Figure 1.2: An exploded view of the DANDE spacecraft assembly. Attitude subsystem components are highlighted.

of electromagnetic interference between components. For example, within the ADC system, this is particularly a concern when using a magnetic torque system in conjunction with a magnetometer measuring the Earth's geomagnetic field.

The spherical shape constraint of DANDE also limits the solar cell design, severely limiting the power budget. All subsystems are subject to a tighter than normal Wattage and depth of discharge constraint. This imposes duty cycles on many of the power-hungry components. In the case of the ADC system, this particularly applies to the magnetic torque system.

The nature of the launch opportunity also drives many aspects of the design. DANDE is competing in the University Nanosat Five competition, sponsored by the

Air Force Research Laboratory (AFRL). The Nanosat program awards a launch to the winning entry as a secondary payload aboard an existing Air Force launch. The spacecraft's manifest as a secondary payload carries a number of challenges. First, the spacecraft is subject to a strict set of regulations to mitigate any possible risk it could pose to the primary payload. Second, since the primary payload dictates the orbit to which the launch vehicle will travel, it forces the spacecraft to be designed to a broad spectrum of orbits. Thirdly, and most important to the ADC subsystem, the separation system which detaches the secondary payload from the launch vehicle puts the spacecraft into an unknown initial attitude condition. Some information is available on the upper bounds of the "tip-off" rate, but no information on the orientation of the spacecraft at separation is provided. The ADC system must be designed such that it is operable with undetermined initial attitude and angular rates.

Other challenges to the subsystem are common to most student satellite projects. The budget is extremely limited compared to most government and commercial programs. Technical expertise is very limited, and because students may have never participated in a spacecraft design effort before, extra time must be budgeted to allow students to learn the necessary skills during the course of the project. Many of the facilities necessary to produce a flight-worthy spacecraft are not available on the University campus, for example, a thermal vacuum chamber large enough to test the integrated spacecraft. Other facilities, such as machine shops, are available on campus, but the project must produce and train its own labor. These constraints generally place a premium on the simplicity of a design. The ADC system must be designed to minimize the effort needed to manufacture, test and integrate the subsystem.

This thesis documents the design of an attitude system subject to these constraints. A systematic, top-down systems engineering approach is taken throughout the design process. The end product is an applied, practical solution to a real spaceflight opportunity.

This document follows the top-down systems engineering approaching used to design the ADC subsystem. First, heritage missions with attitude requirements similar to DANDE are reviewed. The DANDE mission itself is then described in greater detail. The architecture trade study (the first major section of work) is then presented. The findings of the trade study produce component level requirements, to which the torque rods and nutation damper are then designed. An attitude simulation tool is then developed for use in the analysis sections. This tool is used to perform the spinup analysis, the second major section of work. In the final major section of work, a study is performed to find the minimum quantity of horizon crossing indicator data needed to meet the attitude determination requirements.

Chapter 2

Literature Review

At the beginning of the DANDE ADC subsystem design process, a number of heritage missions were identified and studied based on similarities to the DANDE mission. Student and university projects were of particular interest. The DANDE project is subject to many constraints common to student satellites, most notably small budgets, limited technical expertise, and shared integration and test facilities.

An excellent example of a student satellite project is FalconSAT-3 out of the US Air Force Academy. The ADC system for FalconSAT-3 was designed and documented by Andrew D. Anderson in 2004[1]. This spacecraft employs a combination of active and passive control to achieve 3-axis stabilization. Stability and control are obtained using a six-phase approach. Separating ADC activities into phases proved to be a useful strategy to the DANDE mission as well.

In Phase 1 of the FalconSAT-3 mission, the spacecraft is assumed to be in a random tumble after separating from the launch vehicle. At this point, only spin *rate* determination is performed and only the magnetometer is utilized. A Kalman filter is implemented to recover spin rate information from noisy 3-axis magnetometer data. In Phase 2, a "B-dot" control law is used to damp rotation rates about the x and z body axes, and to bring the rotation rate about the y-axis to a given reference value.

The B-dot control law is an active control algorithm to stabilize a randomly tumbling spacecraft and bring it to rest with respect to the local magnetic field vector. The

algorithm monitors the Earth's local magnetic field B in the direction of one magnetic torque rod fixed to the body frame, takes the body-fixed first derivative $\dot{B}$ (hence the name "B-dot"), and creates a magnetic dipole in the opposite direction. This acts to create a magnetic torque opposing the current rotation of the spacecraft. Conversely, creating a dipole in the same direction as $\dot{B}$ acts to accelerate a body. Anderson notes that the B-dot control law is only useful at spin rates where the body is rotating much faster than the orbital angular rates.

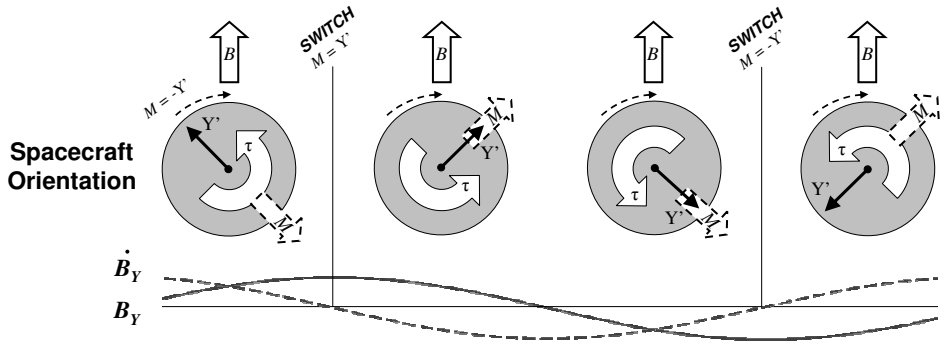

Figure 2.1: The B-dot control law concept. As the spacecraft rotates so that the y-axis more closely aligns with the Earth's B field, the first derivative of the B-field in the y direction is positive. The y-axis torque rod creates a magnetic dipole in the -y direction. By $\tau = M \times B$, a torque opposing the spin rate is generated. The dipole direction is reversed when the y-axis passes the B field direction and $\dot{B}_Y$ becomes negative.

To finish Phase 2 of the FalconSAT-3 attitude control activities, the y-axis is aligned with the orbit normal direction. Anderson refers to this attitude state as a "Y-Thompson" spin mode. The y-axis spin rate is chosen such that, when a boom is deployed along the z-axis in a later phase, the y-axis spin rate coincides with the angular change of the spacecraft in orbit about the Earth. In a nearly circular orbit, this conveniently fixes the spacecraft body axes to the orbit tangent-normal-radial (TNR) reference frame. If deployed with the boom pointing to nadir, the gravity gradient restoring forces stabilize the system as well. Phase 3 extends determination from rates to include attitude knowledge, and the boom is deployed in Phase 4. Phase 5 damps

residual libration after boom deployment and Phase 6 monitors angular deviations during payload operations.

The B-dot control law has been used on a number of successful missions. Another example is AAUSAT-II, built by Aalborg University, Denmark[6]. This 10 cm x 10 cm x 10 cm pico-class satellite uses this algorithm to bring the spacecraft to inertial rest in all three axes after being ejected into a random tumble by the launch vehicle. The paper by Larsen also describes the difficulties encountered when magnetic fields from the torque rod actuators interfere with magnetometer data, a problem also anticipated with the DANDE mission due to volume constraints. Larsen describes the sense/actuate duty cycle and data filtering used on the AAUSAT-II magnetometer, and discusses the effectiveness of these techniques. Unlike FalconSAT-3, AAUSAT-II employed a simple low-pass filter instead of the more computationally-intense Kalman.

Another mission applicable to the DANDE ADC subsystem is the Student Nitric Oxide Explorer (SNOE), designed and built by the Laboratory for Atmospheric and Space Physics (LASP)[13]. While larger and more expensive than DANDE, SNOE has similar payload pointing requirements and is predominantly built by students. This mission in particular was studied extensively not only due to its similar attitude requirements, but also because the availability of mission documentation and personnel. Dr. Tim Holden, the ADC design lead for SNOE, has acted as a mentor for the DANDE project since its inception.

The SNOE spacecraft spins at a nominal 5 RPM about the orbit normal vector, coincident with its major principal axis. This stabilization method was chosen not only for the convenient property that the payload scans through the velocity direction at all points in the orbit, but also for its dynamic properties. By spinning about the principal moment of inertia vector, a near-rigid body spacecraft becomes passively stable and will reject small disturbance torques[11]. Attitude determination on SNOE is performed with two Horizon Crossing Indicators (HCIs) and one 3-axis magnetometer. Active attitude

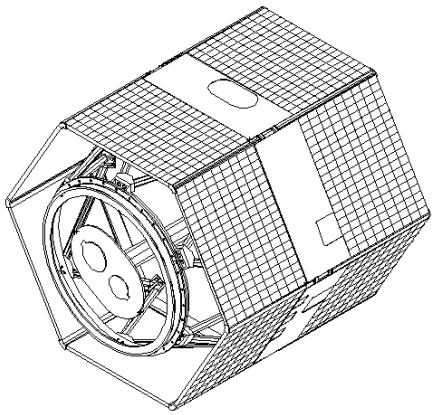

Figure 2.2: The Student Nitric Oxide Explorer (SNOE).

control is done with two ferromagnetic core torque rods, one parallel to the spin axis and one in the transverse direction. A passive nutation damper is used in the form of a fluid-filled ring. Unlike DANDE, SNOE is co-manifested as the primary payload aboard its launch vehicle (an Orbital Sciences Pegasus XL rocket), which spun the spacecraft up to its nominal rotation rate before separation. As such, SNOE was not designed to perform a spin-up maneuver beyond small spin rate corrections.

To perform determination, SNOE employs to Horizon Crossing Indicators (HCIs)[5]. These small field-of-view (FOV) optical sensors send a pulse to an onboard computer every time their FOV moves across the Earth's horizon. These time stamps are used to determine the rate at which the spacecraft is spinning, and the ratio of the time the sensor is pointed at the Earth vs. the sky. This ratio defines the "chord-length" of the Earth, which is a function only of altitude and angle between nadir and the spacecraft spin axis. If the altitude is known from the orbit ephemeris, the HCI data can be used to find the spin-axis angle to nadir. If it can be assumed that the spin axis moves very little over the course of an orbit, angles to nadir over a spread of points in orbit may be used to fully resolve the direction of the spin axis.

This determination methodology is used on a number of spin-stabilized missions,

including the Interplanetary Monitoring Platform (IMP) missions 6, 7 and 8, the Radio Astronomy Explorer 2 (RAE-2) and the Small Scientific Satellite 1 (SSS-1). These missions were all date to the early 1970's, demonstrating this architecture's ability to operate without extensive onboard computing power. This is a great advantage for a mission subject to the technological and development constraints of a student satellite.

HCIs are not the only instrument capable of performing attitude determination on spinning satellites. A number of small spin-stabilized missions have tracked the Earth's magnetic field and the sun vector. The University Satellite (UNISAT), a 20 kg octagon developed at the University of Rome, proposed to use the energy-collecting solar panels of the spacecraft to track the direction of the sun, removing the need for a set of dedicated sun sensors[10]. This strategy is attractive to student projects, in that it would reduce both sensor cost and integration complexity. However, a number of issues make this configuration less attractive to DANDE. First, Santoni's simulation shows that the best performance of the system will determine the spin axis alignment to just under 1.0°, which just barely meets the DANDE requirements. Also, the proposed architecture is demonstrated only in simulation, and no flight data is available to verify whether the deployed system meets its predicted performance. DANDE spins at 10 RPM, twice the rate of UNISAT, and it is unclear how the increased rate will affect determination accuracy. Santoni also recognizes that the weight and complexity savings of removing the sun sensors are somewhat offset by the added computational complexity of developing and integrating a Kalman filter into the attitude determination software. It is also worth noting that this system is operationally constrained to performing attitude determination while the spacecraft is not in eclipse, which is inconvenient for DANDE's sun synchronous, noon-midnight orbit with an apogee of 350 km.

All major-axis spinning spacecraft experience a coning motion of their spin axis about their angular momentum vector called "nutation." This motion causes the spacecraft to "wobble" about a vector fixed in inertial space and must be accounted for in the

pointing error budget. In a minimum energy spin, a rigid body will spin purely about its major axis. Therefore, one common method of reducing the cone of nutation is to use a passive damping device to dissipate kinetic energy from the system without exchanging angular momentum with the surrounding environment. Passive devices are attractive design options for a student project because they do not require interaction with the electrical or computer subsystems, alleviating algorithm development and testing cost, not to mention operational risk.

As mentioned previously, SNOE uses a fluid-filled ring nutation damper. This device is mounted with the ring axis perpendicular to the spacecraft major moment of inertia, so that any rotation out of alignment with that axis causes the fluid to experience a motion relative to the walls of the tube. Energy is dissipated through the viscous forces within the fluid as the bulk mass is accelerated by the moving tube walls.

Other passive devices have been flown with success. Sen[12] proposes and analyzes the concept and Tossman[16] documents the flight performance of a torsional pendulum used to damp nutation on the Small Astronomy Satellite-A (SAS-A). This pendulum is not the canonical point mass on a long arm; it is a passive flywheel mounted perpendicular to the spacecraft spin axis with a torsional restoring device on its axle. SAS-A is about three times as massive as DANDE, and is a dual-spinning spacecraft, however at points in the mission the reaction wheel is stopped and the spacecraft operated as a single rigid body. Although a torsional pendulum is considered a passive device, SAS-A installed active controls to allow for on-orbit tuning of various parameters, such as spring constant and pendulum length. What results is a detailed analysis of on-orbit data with respect to a range of different parameters.

Despite fight heritage on such systems, torsional pendulums and motor/flywheel assemblies are not a favorable design option for DANDE due to the mechanical vibrations induced in the system. DANDE's science payload includes six accelerometers sensitive down to the nano-g scale. Any structural vibration in the system biases or

corrupts these measurements. It is decided early in the design process to eliminate any mechanically dynamic parts from the DANDE structure.

Chapter 3

Background: The DANDE Mission

The Drag and Neutral Density Explorer (DANDE) is a mission to perform in-situ measurements of atmospheric density and wind at altitudes between 100 and 350 km above sea level and to relate this data to drag forces on satellites. The project is a joint effort between the Colorado Space Grant Consortium (COSGC) and the Aerospace Engineering Sciences department at the University of Colorado at Boulder. DANDE is a competing entry in the University Nanosat Five (NS5) Program, sponsored and administrated by the Air Force Research Laboratories. The University Nanosat program awards launch opportunities to student-developed projects based on sound technical products and mission relevance to Air Force scientific interests.

Atmospheric drag plays a major role in the design of low Earth orbiting spacecraft and their operating procedures. For spacecraft in Low Earth Orbit (LEO), atmospheric drag causes perturbations in both attitude and orbit. Attitude perturbations pose a risk to mission pointing requirements, and disturbances must be rejected. Usually this is accomplished with active attitude control, which use up system resources such as power or propellant. Looking at orbit parameters, atmospheric drag will slow the ground speed of the spacecraft, causing it to move to a lower orbit until it completely reenters. Like attitude perturbations, orbit perturbations are usually corrected with active control. Orbit adjustments usually require the spacecraft payload operations to halt while maneuvers are being performed, so these events must be planned and carefully

managed to keep the payloads online and producing data for as long as possible. Both the density of the atmosphere and local winds affect the amount of drag on a satellite, and both vary greatly over the course of even a single orbit. Accurate wind and density forecasting is essential to effectively planning mission operations for LEO spacecraft. This includes a range of operations from formation flying to collision avoidance to re-entry dynamics.

Theoretical models exist for predicting variation in the density and winds of the upper atmosphere, however these models have been shown to deviate as much as 20% from measured values. There exists a need for in-situ data to verify and improve these models. This is the thrust of DANDE's Mission Statement and Primary Objectives.

Table 3.1: The DANDE Mission Statement and Primary Objectives, as seen in the Requirements Flow Down.

Type	Description
Mission Statement	Explore the spatial and temporal variability of the neutral thermosphere at altitudes of 350-100 km, and investigate how wind and density variability over 500-3000 km scales translate to drag forces on satellites.
Primary Objective	Establish and understand the relationship between total mass density, composition, and winds as functions of latitude, level of magnetic activity, and horizontal scale.
Primary Objective	Establish the relative contributions of density and winds to satellite drag as a function of latitude, level of magnetic activity, and horizontal scale.
Primary Objective	Demonstrate key technologies for performing in-situ measurements of the orbital drag environment at low cost.
Primary Objective	Improve understanding of the variation in coefficient of drag in the 100-200 km altitude region.

The Primary Objectives are translated into specific mission-level requirements at the 0.SYSX level. These requirements are listed in Table 3.2.

Obtaining this data from existing satellites is difficult for a number of reasons:

- Drag from atmospheric density is highly coupled with drag from in-track winds,

Table 3.2: The top-level DANDE mission requirements, as seen in the Requirements Flow Down.

Catagory	Description
In-Situ Measurements	Provide simultaneous in-situ density (number and mass) and composition ($O:N_2$ ratio) data over the duration of at least 5 sudden geomagnetic storms (goal: 1000 hours of data) and 4 periods of quiet geomagnetic conditions at an altitude of 350 km (and below) and covering a minimum latitude of at least 54 degrees (goal: polar region coverage from a 350 km sun-synchronous noon-midnight orbit). Store density data with a spatial resolution of density variations of 500 km along the orbit (goal: 250 km).
Tracking and Calibration	Calibrate near real-time models by tracking and evaluate empirical and first-principles models. Estimate the coefficient of drag in orbit at 350 - 100 km altitude.
Winds	Measure the winds at an altitude of 250 km and below (goal: 350 km and below) and at latitudes of at least 54 degrees. Collect wind data over the duration of at least 5 geomagnetic storms and 4 periods of quiet geomagnetic conditions (goal: 1000 hours of data). Provide the wind data with a spatial resolution of at least 50 km (goal: 10 km).
Large Scale Structure	Measure large-scale horizontal variations with in-situ density data over the course of at least 5 geomagnetic storms and 4 periods of quiet geomagnetic conditions (goal: 1000 hours of continuous data).
Key Technologies	Develop a low-cost system to make in-situ measurements of the neutral atmosphere and adhere to all Nanosat Program Requirements. Design, test, and build the proto-flight system for under $100,000 and deliver a proto-flight unit by January 2009

and acceleration measurement alone cannot distinguish between the two

- Drag force varies with the coefficient of drag, which is a function of the cross-sectional area of the spacecraft. This introduces additional coupling of drag force with the attitude of the spacecraft

- Due to the expense of orbit correction maneuvers to mission planning, few

missions fly at altitudes below 350 km, an area of particular interest for re-entry dynamics

DANDE implements an inexpensive and robust method of overcoming these challenges, first proposed by Moe[8]. The concept stems from the equation for atmospheric drag:

$$a_{\text{drag}} = \frac{1}{2} C_D \frac{A}{m} V_i^2 \rho \tag{3.1}$$

where a_{drag} is the acceleration of a body due to atmospheric drag, C_D is the body's coefficient of drag, A is the cross-sectional area of the body with respect to the freestream direction, m is the body mass, V_i is the airspeed of the body, and ρ is local atmospheric density. Before the launch of the DANDE spacecraft, three of these variables are known: m, C_D, and A. The spacecraft mass m will be directly measured. The spacecraft is designed to be spherical, so that cross-sectional area A can also be directly measured and is constant regardless of the attitude of the spacecraft relative to the freestream direction. Likewise, the surface of the sphere is designed such that C_D is well characterized prior to launch and is also insensitive to spacecraft attitude. This leaves only V_i and ρ as unknown variables determining a_{drag}.

DANDE carries an accelerometer payload to measure the drag force a_{drag}, but also carries a Wind and Temperature Spectrometer (WATS) payload. This spectrometer measures the flux of uninoized gas particles through its aperture, which relates directly to $V_i \rho$. In other words, the flux of particles through an aperture scales varies linearly with both density and velocity. However, as seen in Eq(3.1), acceleration due to drag varies linearly with density and with the *square* of velocity. Thus, by collecting acceleration and flux data simultaneously, DANDE will be capable of discerning between density and wind velocity. Additionally, DANDE's spherical shape and low surface-area-to-mass ratio allow it to stay aloft for longer and at lower orbits than larger, less

uniformly shaped satellites.

This system architecture imposes a number of requirements on the attitude knowledge and control of the spacecraft. These appear at the 1.SYSX level of the requirements flow down, shown in Table 3.3.

Table 3.3: The system level requirements on attitude determination and control, as seen in the Requirements Flow Down.

Req. Number	Description
1.SYS25	The spacecraft body axes shall be determined to $\pm 2^\circ$ precision (1-sigma) with respect to the ECI reference frame during science measurements.
1.SYS44	The spacecraft body axes shall have an offset from their nominal ECI vector of no more than $\pm 5^\circ$ during measurements
1.SYS54	In-situ density, composition and mass-flux measurements shall have an associated attitude state corresponding to the same time within ± 5 milliseconds or less.

With the system level requirements on attitude specified, the Attitude Determination and Control (ADC) subsystem is formed. This subsystem is tasked with satisfying all system level requirements relating to the spacecraft's orientation in space.

This work documents the process to design and specify all ADC hardware and algorithms, following a the systems engineering approach.

Chapter 4

Subsystem Requirements and Architecture Design

The first step taken in designing the ADC subsystem is to flow the system level requirements down to subsystem level requirements. The key performance parameters of the ADC subsystem are shown in Figure 4.1.

Table 4.1: Subsystem level requirements on the performance of the ADC subsystem, as seen in the Requirements Flow Down.

Req. Number	Description
2.ADC1	The Attitude Determination and Control (ADC) subsystem shall achieve its final attitude state within 144 hours (six days) of subsystem activation.
2.ADC3	The ADC subsystem shall determine the attitude of DANDE with respect to the velocity or cross-track directions to within 2° during density measurement cycles.
2.ADC4	The ADC subsystem shall bring the science measurement sensors within a 5° half-cone of the velocity vector at a rate no slower than 1 time per minute and no faster than 20 times per minute.
2.ADC10	The ADC subsystem shall have a peak power no greater than 7.5 W, in accordance with the power budget UN5-SYS114.
2.ADC16	The ADC subsystem shall not exceed 6.00 kg of mass allocated to it in UN5-SYS111.
2.ADC17	The ADC subsystem shall not contain pressurized components.
2.ADC19	The ADC subsystem shall remain operable to 4.7 rad of Total Ionizing Dose over 400 days.
2.ADC20	The ADC subsystem shall remain operable in the EMI and RFI environment of the on-orbit DANDE spacecraft.

In addition to the key performance requirements on the ADC subsystem, there are a number of requirements imposed on the subsystem design by other subsystems. These requirements assure that the subsystem adheres to the mass budget, power budget, radiation requirements, and other systems engineering issues.

Table 4.2: Systems engineering requirements on ADC, as seen in the Requirements Flow Down.

Req. Number	Description
2.ADC10	The ADC subsystem shall have a peak power no greater than 7.5 W, in accordance with the power budget UN5-SYS114.
2.ADC16	The ADC subsystem shall not exceed 6.00 kg of mass allocated to it in UN5-SYS111.
2.ADC17	The ADC subsystem shall not contain pressurized components.
2.ADC19	The ADC subsystem shall remain operable to 4.7 rad of Total Ionizing Dose over 400 days.
2.ADC20	The ADC subsystem shall remain operable in the EMI and RFI environment of the on-orbit DANDE spacecraft.

After these "Level 2" requirements were established, the next step in the design process is to use these requirements to establish a subsystem architecture.

A decision tree is used to help weigh the options for the subsystem design architecture. The tree is shown in Table 4.1. Decisions are made in order from left to right.

4.1 Attitude Stabilization

The highest level design trade done in the ADC subsystem trade study is the method of stabilization. 3-axis control, spin stabilization, and gravity gradient systems are all considered, however gravity gradient stabilization is quickly eliminated and does not appear in the study. Gravity gradient stabilization is typically done with masses on long booms, and the spherical shape requirement on the sphere rules out this option.

Attitude Determination and Control System Trade Tree (July 1, 2007)

	S/C Stabilization	Control Method	Sensors	Actuators
ADCS System	Three-axis stabilization	Open Loop (on ground)	sun sensors	magnetic torque rods/coils
			magnetometer	reaction wheels
			horizon sensors	CMGs
			star trackers	thrusters
			IMU	nutation damper
		Closed Loop (on board)	sun sensors	magnetic torque rods/coils
			magnetometer	reaction wheels
			horizon sensors	CMGs
			star trackers	thrusters
			IMU	nutation damper
	Two-axis stabilization (spinner)	Open Loop (on ground)	sun sensors	magnetic torque rods/coils
			magnetometer	reaction wheels
			horizon sensors	CMGs
			star trackers	thrusters
			IMU	nutation damper
		Closed Loop (on board)	sun sensors	magnetic torque rods/coils
			magnetometer	reaction wheels
			horizon sensors	CMGs
			star trackers	thrusters
			IMU	nutation damper

Figure 4.1: Decision tree evaluated in the ADC architecture trade study. Decisions are made from left to right.

4.1.1 Three Axis

Three-axis stabilization is complete control of the spacecraft's orientation along all three axes. This is the typical configuration of higher-end, more expensive satellites with dynamic pointing requirements. It requires closed loop control and is usually very computationally intense. Benefits include the capability to have the spacecraft autonomously track any arbitrary pointing requirement and a huge flexibility of maneuvers the spacecraft is capable of performing.

4.1.2 Spin Stabilization

Spin stabilization maintains control of the spacecraft by spinning it like a top, then controlling the orientation of the axis of rotation. It is typical of lower-cost satellites with "scanning" pointing requirements. Because any semi-rigid body will eventually decay to spin about its major axis due to energy dissipation, it usually imposes strict requirements on the mass properties of the spacecraft. Once the spacecraft is spun up and nutation is damped from the spin, the angular momentum of the rotation helps to reject disturbance torques. It is a typically a much simpler, less expensive design than three-axis stabilization, but forces the payload to be in constant rotation.

Each issue considered when selecting a stabilization design option is presented in Table 4.3. A zero through five weighting factor is assigned to each issue to rank its importance to the success of the DANDE mission.

Each of the issues presented in the previous section are compared to the two design options in question. Each option is given a zero to five score assessing how well the option accommodated the issue. The scores are multiplied by each issues' weighting factor to come up with a weighted score, which is used to compare the adequacy of each design choice to the application at hand. Data is tabulated in Table 4.4.

Table 4.3: Discussion of issues involved with methods of spacecraft stabilization and weighting factors assigned to each issue.

Factor	Discussion	Weighting Factor
Fidelity of science data	Three axis stabilization points the science payloads in the ram direction for all of the data taking portion of the mission. Spin stabilization requires "scanning" of the ram direction, but also allows points the accelerometer to point in the anti-ram direction. This would allow for real-time bias removal on the accelerometer.	5
Operational risk	Three axis stabilization requires constant monitoring and closed-loop feedback control. If there is any hardware or software failure, a work-around would have to be developed before the mission could continue. Spinning spacecraft deviate more slowly from their nominal attitude in a given disturbance environment. This allows the craft to be operated entirely open-loop if need be, giving much more flexibility to the operations crew and mitigating the risk to mission success if a failure occurs.	4
Ease of software design	Three axis stabilization requires extensive closed loop control algorithm development. Spinning spacecraft require much simpler control algorithms. Development and test schedules place importance on simplistic design.	3
Ease of build and integration	Three axis requires more hardware, more precision integration and calibration, and extensive testing. Spinners require a little as two torque rods and a passive damper.	3
Cost	Three axis requires more hardware and more precision, both on the determination and actuation side. Spinning may require multiple accelerometers to meet sampling rate requirement.	2

Table 4.4: Comparison of weighted scores of each stabilization method.

Factor	Weighting Factor	Three Axis Score	Spin Score	Three Axis Weighted Score	Spin Weighted Score
Fidelity of science data	5	5	4	25	20
Operational risk	4	2	4	8	16
Ease of software design	3	1	4	3	12
Ease of build and integration	3	1	3	3	9
Cost	2	2	3	4	6
Total				**43**	**63**

4.1.3 Discussion

Spin stabilization scores a much higher total weighted score than three-axis stabilization. This is mostly due to the relative simplicity of the spin stabilization scheme compared to three-axis control. For the limited time and resources of a student project, simplicity is important to any design option. With multiple accelerometers, the system should easily meet the data collection time requirement, which is the only issue for which 3-axis stabilization outscores spin-stabilization. This imposes some additional requirements on the structure of the spacecraft, detailed in the Requirements Flow Down: 1) the major principal axis of the spacecraft must lie within a budgeted alignment error of perpendicular to the accelerometer plane, and 2) the major principal axis of the spacecraft must be larger than the next largest principal axis.

DANDE will be spin-stabilized about an axis perpendicular to the accelerometer plane. The rate of rotation and number of accelerometers will accommodate the data collection time requirement 1.SYS5 and 1.SYS65.

4.2 Control Method

4.2.1 Open Loop Control

Open loop control is a method by which the spacecraft's actuation mechanism is not autonomously driven by sensors and an on-board control algorithm. In DANDE's case, the spacecraft's actuation system only responds to commands from a ground station, for example, "turn torque rod X on at time Y and off at time Z." It is the most simple system of control with regards to flight hardware and software. It transfers the computational burden from the spacecraft to the ground station. It is limited in that commanding is only possible when in contact with the ground station. For precision maneuvers, this is especially a problem due to the time needed to sense an attitude, send sensor data to the ground, evaluate the data, formulate a corrective maneuver, and send the command back to the spacecraft.

4.2.2 Closed Loop Control

Closed loop control connects the sensors and actuators in a loop, so that the spacecraft can detect and alter its orientation based on an on-board set of control algorithms without intervention by the ground station. It is the best option for tracking a pointing requirement in a disturbance-rich environment. Compared to open-loop control, it is much more computationally intense, as the spacecraft must have all the "brains" required to determine attitude and formulate corrective maneuvers on-board. However, it is the only way to control attitude when updates to actuator input algorithms are needed more frequently than the spacecraft comes in contact with the ground station.

Each issue considered when selecting a design option is presented. A zero through five weighting factor is assigned to each issue to rank its importance to the success of the DANDE mission. Data is tabulated in Table 4.5.

Each of the issues presented in the previous section is compared to the two design

Table 4.5: Discussion of issues involved with methods of spacecraft control and weighting factors assigned to each issue.

Factor	Discussion	Weighting Factor
Meet pointing requirement	Closed loop control provides a faster response to disturbances. However, the disturbance environment is anticipated to be mild enough to use open loop control effectively	5
Operational risk	Open loop control does not require any changing of on-board software to deal with unexpected behaviors. However, open loop control will not be capable of spinning up the spacecraft. Closed loop algorithms may require no attention if they work as planned, but in the case on an anomaly, software patches can be difficult and time consuming to formulate, upload, and verify.	5
Cross-system stresses	Open loop only requires an interface to the CDH system, which will act as a relay for ground commands. Closed loop control requires an interface to the sensors, filters, a dedicated processor, memory, algorithm, and all the associated watchdog programs	3
Ease of design	Open loop flight software will only require an interface to CDH. Algorithm development will still have to occur, but as a part of the Ground Support Equipment and will not be as time-critical as flight software. Closed loop will require time-critical algorithms to be developed, integrated and tested in flight software.	3
Cost	Closed loop may require only more processing hardware.	2

options in question. Each option is given a zero to five score assessing how well the option accommodated the issue. The scores are multiplied by each issues' weighting factor to come up with a weighted score, which is used to compare the adequacy of each design choice to the application at hand. Data is tabulated in Table 4.6.

Table 4.6: Comparison of weighted scores of each control method.

Factor	Weighting Factor	Open Loop Score	Closed Loop Score	Open Loop Weighted Score	Closed Loop Weighted Score
Meet pointing requirement	5	4	5	20	25
Operational risk	5	2	3	10	15
Cross-subsystem stresses	3	5	2	15	6
Ease of design	3	4	1	12	3
Cost	2	4	4	8	8
Total				**65**	**57**

4.2.3 Discussion

Open loop edged out closed loop in the decision matrix, but not by much. The "Operational Risk" category is by far the most difficult to quantify. The open loop system is far more robust once the spacecraft has been spun-up, but the spin-up maneuver may not be able to be done by open-loop control. Closed loop is maintenance-free if everything works correctly, but banking on that is a huge risk to a student-built mission with such limited time and budget.

The most favorable option seems to be a limited hybrid of open and closed loop methods. The spin-up maneuver is to be be performed using a simple and rigorously tested closed loop algorithm. Once the proper rotational rates are achieved, control

of the orientation of the spin axis is to be performed open loop. This combination of open and closed loop control has flight heritage on the SNOE spacecraft. This limits the number and complexity of closed-loop algorithms needed and places as much of the control as possible in the ground element.

4.3 Sensor Selection

To perform attitude determination, five common sensors for spacecraft are considered: sun sensors, magnetometers, horizon crossing indicators, star trackers, and inertial measurement units. Each option is discussed individually.

4.3.1 Sun Sensors

Sun sensors provide the spacecraft with the azimuth and elevation of the sun vector, giving one axis of attitude knowledge. To attain full attitude knowledge, a sun sensor must be combined with at least one other instrument to resolve the rotation ambiguity about the sun vector direction. A low-end sun sensor can provide 5° of pointing knowledge, and finer instruments down to less than 1° are available at an increased cost. Because these sensors require an unobstructed view of the sun, at least two sensors must be mounted on opposite sides of the spacecraft for full coverage, and no data will be collected while the spacecraft is in eclipse. Also, sun sensors may not be effective at high rates of spin. They are usually available in one and two axis varieties, e.g. azimuth, elevation, or both[7].

4.3.2 Magnetometers

Magnetometers measure the Earth's magnetic field vector local to the spacecraft. Most magnetometers come as a three-axis package that outputs three orthogonal components of the magnetic field, however single axis magnetometers are also available. Magnetometers are sensitive enough to pick up eddy currents on spacecraft, so care

must be taken to separate spacecraft-induced magnetic fields from the Earth's magnetic field. Accuracy is usually limited by spacecraft noise and data is good even at high rotation rates, provided that the sampling frequency is high enough[7].

Like sun sensors, magnetometers must be used in conjunction with another instrument due to the attitude ambiguity about the detected vector. Magnetometers are mass produced and relatively inexpensive.

4.3.3 Horizon Crossing Indicators

Horizon Crossing Sensors (HCIs) are optical instruments that activate a detector when the sensor is pointed at the Earth. They work by signaling a "crossing" when the sensor detects a change in the amount of infrared radiation in its field of view. By tuning the detector to the infrared band emitted by carbon dioxide, HCIs indicate the time the sensor boresight crosses the Earth's horizon. The relative time interval between crossings can be used to gauge the deviation of the spin axis from orbit normal, in this mission referred to as "roll". If roll data is taken over several points in orbit, it can be post-processed to determine the spin axis vector in inertial space. Because HCIs supply one data point every time their boresight crosses in or out of the Earth's horizon, HCIs are more effective with spacecraft that rotate at higher rates[7].

Note that Horizon Crossing Indicators differ from Earth Sensors in that they are designed specifically for spinning spacecraft. Earth sensors also detect the $C0_2$ "limb" of the Earth, but they require the horizon to be nearly stationary within their field of view to determine angle to the horizon.

4.3.4 Star Trackers

Star trackers determine attitude by taking a picture of the sky and mapping it against a catalogue of known star positions. They are very precise, but also the most expensive attitude determination instrument. They are not typically used on spinning

spacecraft, as high rotation rates can make the picture blurry[7].

4.3.5 Inertial Measurement Units

Unlike the other sensors considered, Inertial Measurement Units (IMUs) do not detect the absolute attitude of the spacecraft relative to its environment. IMUs are used to detect changes in rates of rotation with a high degree of precision. By integrating the rates of rotation over time from a known position, IMUs allow the spacecraft to propagate its attitude when data from other attitude sensors is infrequent. However, attitude propagation tends to be computationally intense. It is also imperative that the state of the system be updated periodically from other instruments, as attitude propagation from IMUs will drift over time[7].

Each issue considered when selecting a design option is presented. A zero through five weighting factor is assigned to each issue to rank its importance to the success of the DANDE mission. Data is tabulated in Table 4.7.

Each of the issues presented in the previous section is compared to the two design options in question. Each option is given a zero to five score assessing how well the option accommodated the issue. The scores are multiplied by each issues' weighting factor to come up with a weighted score, which is used to compare the adequacy of each design choice to the application at hand. Data is tabulated in Table 4.8.

4.3.6 Discussion

The magnetometer and HCIs came out well ahead of the other sensors in the decision matrix. This is due mostly to their ability to operate accurately at high rotation rates. The magnetometer is required for a closed-loop spin up maneuver based on the B-dot control law.

The system might function without horizon crossing indicators. However, there is significant risk in having only a single attitude determination sensor. In the case of

Table 4.7: Discussion of issues involved with attitude sensor and weighting factors assigned to each issue.

Factor	Discussion	Weighting Factor
Determination accuracy	The sensors must have the resolution and accuracy to meet the knowledge requirement. Specifically, the suite must determine the orientation of the spin axis in ECI coordinates, the phase angle and rotation rate to the acceptable limits of the error budget.	5
Ease of integration and test	The sensor suite and determination algorithms must be integrated and tested to the requirements of the ADC subsystem within the bounds of the schedule.	5
Cost	Sensor cost must be kept to a minimum, as they are potentially high-dollar items.	4
Operational risk	The sensor suite must be robust. Wherever possible, the determination system must be fault tolerant (i.e. a workaround should be manageable should any single sensor fail).	4
Cross-system stresses	The sensors should not interfere with the normal operation of any other subsystem. This includes any undue stress on the power, thermal or computation budget.	3

a sensor failure, there could be no workaround. The HCIs are particularly well-suited orbit normal spinning spacecraft and provide better timing data than the magnetometers might. In a complete magnetometer failure, it may be possible to come up with a spin-up algorithm using the HCIs.

This sensor suite configuration has flight heritage on SNOE.

4.4 Actuator Selection

Five common spacecraft attitude actuators are considered: magnetic torque rods or coils, reaction wheels, control moment gyroscopes, thrusters and passive nutation dampers. Each actuator is discussed individually.

Table 4.8: Comparison of weighted scores of each attitude sensor.

Factor	Weighting Factor	Sun Sensor Score	Magnetometer Score	HCI Score	Star Tracker Score	IMU Score	Sun Sensor Weighted Score	Magnetometer Weighted Score	HCI Weighted Score	Star Tracker Weighted Score	IMU Weighted Score
Determination Accuracy	5	2	5	5	1	0	10	25	25	1	0
Ease of Integration and Test	5	4	4	4	5	3	20	20	20	25	15
Cost	4	3	5	4	1	3	12	25	20	4	12
Operational Risk	4	4	4	4	0	3	16	16	16	0	12
Cross-System Stresses	3	5	4	4	4	5	15	12	12	12	15
Total							**73**	**98**	**93**	**42**	**54**

4.4.1 Magnetic Torque Rods/Coils

Magnetic torque is a simple and very common mechanism of angular momentum exchange for satellites in LEO. By running current through a coil of wire, a magnetic field is generated. This field interacts with the Earth's magnetic field and creates a torque acting to bring the two into alignment. By reversing the current in the wire, the magnetic field is reversed and therefore so is the torque. Torque rods work the same way a coil does, but using a ferromagnetic core to amplify the field created. The torques are typically small and require a sustained current to generate usable rotation rates. The torque is also dependent on the strength and local orientation of the Earth's magnetic field, so at least a coarse knowledge of the orbit and Earth's magnetic field is necessary for performing three axis maneuvers[7].

4.4.2 Reaction Wheels

Reaction wheels create torque on a spacecraft by applying an opposite torque on a flywheel, changing its spin rate. By accelerating or decelerating the speed of the wheels, the motors may apply a torque on the spacecraft in either direction about the axis of the wheel. They are capable of providing higher torques than magnetic torque rods, but are more power intense, more expensive and prone to mechanical failure. Three wheels provide complete three-axis control of a spacecraft, though most three-axis stabilized craft carry at least four wheels for redundancy.

Reaction wheels are never flown as the sole attitude actuation device on a spacecraft. The reaction torque used to adjust attitude is an exchange angular momentum with the spacecraft body, but not with the outside environment. A persistent disturbance torque in the same direction will constantly add angular momentum to the system, and a reaction wheel would have to be perpetually accelerated to reject the torque on the body. Because reaction wheels are limited in how fast they can spin,

they are not a sufficient momentum management system for a spacecraft. Reaching a maximum wheel speed is known as "saturation" and some other mechanism must be used to "desaturate" the wheels, meaning exchange momentum with the surrounding environment[7].

Reaction wheels on the DANDE spacecraft would need to be implemented in conjunction with magnetic torquers or thrusters. This is an unattractive option as it would double the active actuation components on board, stressing the mass, power, and computing budgets, as well as adding development time for a more complex system.

4.4.3 Control Moment Gyroscopes

Control Moment Gyroscopes (CMGs) re-orient a spacecraft by storing angular momentum in a fast spinning, heavy flywheel, then moving its spin axis to impart a torque on the spacecraft. CMGs are capable of very large, precise torques, but are heavy, expensive and power intensive. They are generally used only on three-axis stabilized craft with very stringent and dynamic pointing requirements[7].

4.4.4 Thrusters

Thrusters expel mass from the spacecraft into the surrounding environment, creating a reaction force. To control attitude, they are arranged in couples, pointing opposite each other and located on a line passing through the spacecraft's center of mass. They are capable of large, coarse torques, but unlike the actuators listed so far, are also capable of creating a net force on the spacecraft. Therefore, thrusters are capable of changing the spacecraft's orbit if coupled thrusters are not precisely paired. UN5 highly discourages the use of thrusters as the pressurized tanks are dangerous to work with and pose an increased risk to the primary payload[7].

4.4.5 Nutation Dampers

Nutation dampers are generally passive devices that dissipate the kinetic energy of periodic rotations of a spacecraft in a specific direction. They are used to more rapidly decay a spin-stabilized spacecraft into pure spin about the major principal axis. One common and simple device is the fluid-filled ring damper. Conceptually, this resembles a bike tire filled with some viscous fluid. When accelerated about the central axis of the ring, the viscosity of the fluid resists a change in spin rate by creating drag on the walls of the ring. By placing the damper such that the central axis of the ring is perpendicular to the major principal axis, any component of the rotation vector **not** on the major access will cause the ring to go into motion relative to the contained fluid, causing energy dissipating drag and eventually eliminating nutation about the major axis[4].

Fluid-filled ring dampers must be "tuned" to the expected nutation frequency of the spacecraft. They must also be designed to allow for thermal expansion of the fluid without rupture[4]. Energy dissipation is inevitable in any body that is not perfectly rigid, so in many applications a nutation damper may not be necessary.

Other passive damper designs include a rolling ball in a tube, mass on a flexible beam, or other mechanically dynamic parts. These are undesirable to the DANDE mission due to their interference with the science payload. Small vibrations or change in Center of Gravity (CG) of the spacecraft will be detected by the accelerometer payload and distort the drag data.

Each issue considered when selecting a design option is presented. A zero through five weighting factor is assigned to each issue to rank its importance to the success of the DANDE mission. Data is tabulated in Table 4.9.

Each of the issues presented in the previous section is compared to the two design options in question. Each option is given a zero to five score assessing how well the

Table 4.9: Discussion of issues involved with attitude actuators and weighting factors assigned to each issue.

Factor	Discussion	Weighting Factor
Capability to meet pointing requirement	Actuators must have the precision necessary to bring the major principal axis of the spacecraft to within the budgeted error (5°) of orbit normal.	5
Capability to meet spin-up requirement	Actuators must have the capability of accelerating the spacecraft from a worst-case initial attitude state to the nominal spin rate in the budgeted time frame.	5
Cross-system stresses	Actuators must be capable of full operation within the allotted power budget. The actuators may not interfere with the proper functions of other systems, especially science, communications and the attitude sensors.	4
Cost	Actuators tend to be relatively expensive components of a spacecraft. The actuator suite must be within allotted monetary budget.	4
Compatibility with control methodology	Actuators must be suited for use during the closed loop spin-up maneuver and open loop alignment maneuver.	3
Ease of integration	Complicated actuators will require many student-hours to integrate, test and verify. A simpler actuator is far preferable.	3

option accommodated the issue. The scores are multiplied by each issues' weighting factor to come up with a weighted score, which is used to compare the adequacy of each design choice to the application at hand. Data is tabulated in Table 4.10.

4.4.6 Discussion

Magnetic torque actuators edged out all other active forms of actuation in the decision matrix. They are attractive to a student project in that they are robust, inexpensive, and simple to integrate and control. DANDE is a small enough craft that even low torques should provide enough actuation, but this assumption must be verified by simulation. Simulation is needed to verify the torque rods will be powerful enough

Table 4.10: Comparison of weighted scores of each attitude actuator.

Factor	Weighting Factor	Mag. Torque Score	Reaction Wheel Score	CMG Score	Thruster Score	Nutation Damper Score	Mag. Torque Weighted Score	Reaction Wheel Weighted Score	CMG Weighted Score	Thruster Weighted Score	Nutation Damper Weighted Score
Pointing Requirement	5	4	5	5	2	0	20	25	25	10	0
Spin-up Requirement	5	4	5	2	5	0	20	25	10	25	0
Cross-System Stresses	4	3	2	0	0	5	12	8	0	0	20
Cost	4	5	3	0	1	5	20	12	0	4	20
Control Method Compatability	3	4	4	0	3	5	12	12	0	9	15
Ease of integration	3	4	2	0	0	5	12	20	0	0	15
Total							**96**	**88**	**35**	**48**	**70**

to perform both the spin-up and alignment maneuvers without exceeding the power, mass or volume budget.

SNOE exclusively used magnetic torque rods for attitude control. The SNOE actuator suite consisted of one rod mounted along the spin axis and one on a transverse axis. The axial rod could be used to control the alignment of the spin axis without affecting spin rate. The transverse rod could spin up the spacecraft without the assistance of the axial rod. Using the open loop/closed loop control algorithms described in Section 4.2, this is the minimum actuator suite needed.

The nutation damper is included in the matrix as an actuator, but it should not be considered a substitute for any active attitude actuation system.

4.5 Archetecture Summary

The DANDE spacecraft will be spin-stabilized about the major principal moment of inertia. The spin axis will be aligned to the orbit-normal direction, with accelerometers mounted to the plane scanning through the ram direction. The maneuver to spin up the craft may be closed loop, but all other maneuvers of the spacecraft will be controlled open-loop. The attitude sensor suite will consist of one three-axis magnetometer to be used primarily for the spin-up maneuver and two HCIs for attitude determination during normal operation. The actuator suite will consist of two magnetic torque rods, one mounted parallel to the spin axis and one perpendicular to it. Additionally, a passive fluid-filled ring nutation damper will be used.

A visual representation of the trades made is seen in the modified tree in Table 4.2.

These architecture design decisions were incorporated into the Requirements Flow Down as Level 3 (Achitecture-Specific) Requirements. The ADC Level 3 requirements are shown in Table 4.11.

Attitude Determination and Control System Trade Tree (July 1, 2007)

	S/C Stabilization	Control Method	Sensors	Actuators
ADCS System	Three-axis stabilization	Open Loop (on ground)	sun sensors	magnetic torque rods/coils
			magnetometer	reaction wheels
			horizon sensors	CMGs
			star trackers	thrusters
			IMU	nutation damper
		Closed Loop (on board)	sun sensors	magnetic torque rods/coils
			magnetometer	reaction wheels
			horizon sensors	CMGs
			star trackers	thrusters
			IMU	nutation damper
	Two-axis stabilization (spinner)	Open Loop (on ground)	sun sensors	magnetic torque rods/coils
			magnetometer	reaction wheels
			horizon sensors	CMGs
			star trackers	thrusters
			IMU	nutation damper
		Closed Loop (on board)	sun sensors	magnetic torque rods/coils
			magnetometer	reaction wheels
			horizon sensors	CMGs
			star trackers	thrusters
			IMU	nutation damper

Figure 4.2: Design decisions made by the ADC architecture trade study.

Table 4.11: Requirements on the ADC architecture, as seen in the Requirements Flow Down.

Req. Number	Description
3.ADC1	The DANDE spacecraft will be designed for spinning around the orbit normal vector in RTN frame.
3.ADC2	The spin rate (magnitude of the spin vector in inertial space) of the spacecraft during science data collection shall be 60 $\pm 12^\circ$ per second.
3.ADC3	The system will command alignment of the spin axis with an open-loop, ground controlled determination and control mode.
3.ADC4	The DANDE spacecraft shall achieve the spin rate magnitude in the X' body axis in a closed loop control mode starting from the following worst-case attitude condition in the nominal orbit: oriented with the Y torque rod perpendicular to the ecliptic and spinning at .1 rad/sec about the body Y-axis.
3.ADC5	The DANDE spacecraft shall achieve its required spin rate within 24 hours of subsystem activation.
3.ADC6	The ADC subsystem shall achieve its required spin axis alignment within 120 hours of subsystem activation.
3.ADC7	The spacecraft maintain spin axis alignment to orbit normal to within 5° half-cone during the science mission lifetime.
3.ADC8	Determination of the spin axis orientation during science collection shall determine the spin axis to a 1° half-angle cone around the true axis orientation with an updated state(s) at least once every 12 hours.
3.ADC9	Determination of the spin vector magnitude shall determination the spin rate to within $\pm 0.5^\circ$ per second at least once every 12 hours.
3.ADC10	Control authority will be achieved with two ferromagnetic-core torque rods, one aligned with the Y' axis and the other aligned with the X' axis.
3.ADC11	Determination during spin up mode will be achieved with magnetometer data.
3.ADC12	Determination during open-loop control mode will use two Horizon Crossing Indicators (HCI's), with the system capable of meeting the determination requirements of 3.ADC8 by operating only one HCI. Goal: utilize the second HCI for determining ambiguous cases and to improve precision, redundancy.
3.ADC17	The DANDE sphere will passively decay to pure spin about the $\pm$X' axis within a 1° half-cone.

Chapter 5

Actuator Design and Specification

Attitude determination and control hardware is designed and specified through a combination of analytical design and reference to heritage missions.

The Level 3 requirements listed in Table 4.11 are decomposed into Level 4 requirements, which place specific requirements on individual components of the subsystem. With these specifications at hand, make/buy decisions are conducted for each component. For components to be purchased, a technical specification document for the vendor is compiled based on the Level 4 requirements. For components to be made in-house, detailed mechanical and electrical drawings are made for component fabrication.

5.1 Torque Rods

The baseline torque rod design is based on the SNOE torque rods. The requirements on the design are validated by simulation in attitude propagation models, and these component level requirements are verified by component-level.

SNOE requires 10 Am^2 of magnetic dipole in order to perform active attitude control. DANDE is a less massive system with a much smaller moment of inertia, however the SNOE active ADC system was only sized to perform small attitude corrections. Therefore, the performance requirement for the baseline DANDE torque rods is set to 7 Am^2.

The core for the SNOE rods is made from CMI-B (ultra low carbon, cold rolled

iron strip). The rod core measures 11.1" in length and 1/4 in diameter. It is wrapped with 4,360 turns of 28 gauge (AWG) magnet wire and activated with 152 milliamps of current.

Using formulas from an Arizona State University technical report used to design torque rods for UASat[9], a spreadsheet is created to design DANDE's torque rods. The spreadsheet takes inputs of allotted power, bus voltage, wire gauge and material properties, and core dimensions and material properties. Using these inputs, it generates the resulting magnetic dipole strength, number of turns, and other physical properties of the system. This spreadsheet is shown in Table 5.1. The final design values appearing here are the result of a collaborative effort with Bradley Brisnehan.

The torque rod design is sensitive to a large number of design parameters. Voltage is regarded as a constant, as the electrical power subsystem required the torque rods to run off the 12V unregulated bus. The power consumption is limited by the power budget, although it is built into the spreadsheet as a user defined variable. Wire thickness is perhaps the most difficult design decision made. A thin wire is limited in how much current it may carry before the insulation begins to break down from the temperature rise. A thicker wire may carry more current, but has less resistance per meter, so a longer length of thicker wire must be used if power consumption is to be held constant. This quickly drives the mass of the assembly beyond the mass budget. Additionally, the wires require derating beyond their typical current carrying capacities due the loss of convective cooling in vacuum.

The values shown in Table 5.1 were arrived at using a derating factor of 0.85. A maximum current was established for every considered wire gauge. A nominal core diameter and length was then defined. Given the core geometery and max current, the number of turns was found based on the required magnetic dipole. From the number of turns and wire gauge, the coil length and resistance can be found, and using $V = iR$, the required voltage to drive the system is found. The gauge of wire was varied until

Table 5.1: Spreadsheet used to design the ferro-magnetic core torque rods.

INPUTS				
Variable	Description	Value	Units	Comment/Source
P	Power	1.096	W	
V	Voltage DC	12.0	V	
r_w	Wire radius	1.13E-04	m	31 gauge wire, M1177
R_s	Electrical resistance, specific	1.70E-08	Ohms·m	copper, cold drawn
ρ_w	Mass density of wire	8960	kg/m^3	copper, cold drawn
l_c	Length of core	0.191	m	$= 7.5$ inches
r_c	Core radius	0.005	m	$= 3/8$ inches diameter
μ_r	Relative magnetic permeability	700	ratio	AISI 416 stainless
ρ_c	Mass density of core	7800	kg/m^3	$= 7.8$ g/cm^3, 416 stainless
μ_0	Permeability of free space	1.25E-06	m·kg/s^2/A^2	constant
OUTPUTS				
Variable	Description	Value	Units	Comment/Source
i	Current	0.091	A	$i = P/V$
R_r	Resistance required	131.39	Ohms	$R_r = V^2/P$
l_w	Length of wire	310.04	m	$l_w = R_r/(R_s/(\pi r_w)$
N	Number of turns	10361	count	$N = l_w/(2\pi r_c)$
n	Layers of wire	13	count	$n = \mathrm{CEIL}(2r_w N/l_c)$
r_T	Total radius of wound rod	7.70E-03	m	$r_T = 2r_c n r_w$
ν_d	Demagnetization factor	6.79E-03	ratio	$\nu_d = \frac{4\ln(l_c/r_c)-1}{(l_c/r_c)^2-4\ln(l_c/r_c)}$
k_1	Dummy variable	0.008	ratio	$k_1 = \nu_d + 1/\mu_r$
m	Magnetic dipole moment	8.21	A·m^2	$m = \pi r_c^2 N i/k_1$
m_w	Mass of wire	0.111	kg	$m_w = \rho_w \pi r_w^2 l_w$
m_c	Mass of core	0.106	kg	$m_c = \rho_c \pi r_c^2 l_c$
L	Inductance	3.77E+03	H	$L = (\mu_0 \pi r_c N^2)/(L_w k_1)$

a voltage near the desired 12 volts was produced. Fine tuning was done by using a goal-seek to increase the magnetic dipole until exactly 12V was obtained as the input voltage.

5.2 Nutation Damper

The fluid-filled ring nutation damper design is based on a paper by Bhuta and Koval in 1966[3]. Bhuta's findings are implemented in a spreadsheet to optimize design parameters to the DANDE mission. The spreadsheet accept inputs of the physical dimensions of the ring, material properties of the fluid, and mass properties of the spacecraft. The inputs are used to find the time constant with which the half-cone of nutation will be reduced on the spacecraft rotating at the nominal 10 RPM. This spreadsheet is shown for the final design of the nutation damper in Table 5.2.

An 8.62 hour time constant refers to the exponential decay of the nutation cone, i.e. after 8.62 hours, the angle between the angular momentum vector $\boldsymbol{H}$ to the cone of nutation has decreased from its original value by 37%. To meet the pointing requirement, the nutation half-cone must decay to $< .1^\circ$ in 96 hours. At this rate of decay, the nutation angle would be reduced from its theoretical upper bound of 90° bound in less than 55 hours. This rate will be verified through simulation.

Table 5.2: Spreadsheet used to design the fluid-filled ring nutation damper.

INPUTS				
Variable	Description	Value	Units	Comment/Source
r_R	Radius to center of ring	0.1	m	flexible
r_{xc}	Radius of cross-section	0.01	m	flexible
ω_S	Spin rate of the spacecraft	0.16667	Hz	10 RPM
ρ	Fluid density	789	kg/m^3	Ethanol @ 20C
ν	Kinematic viscosity of fluid	1.60E-06	m^2/s	Ethanol @ 20C[4]
I_S	Moment of inertia, s/c spin axis	1.01885	kg·m^2	45 kg sphere with $\frac{I_S}{I_T} = 1.15$
I_T	Moment of inertia, s/c transverse axis	0.88555	kg·m^2	45 kg sphere with $\frac{I_S}{I_T} = 1.15$
$f(\gamma)$	Function $f(\gamma)$ from Bhuta[3], Figure 3	0.6	none	dummy variable, update manually
OUTPUTS				
Variable	Description	Value	Units	Comment/Source
V	Volume, fluid	0.0002	m^3	$V = 2\pi^2 r_R r_{xc}^2$, volume of a torus
M	Mass, fluid	0.15574	kg	$M = V\rho$
λ	Inertia ratio	0.15054	ratio	$\lambda = \frac{I_S - I_T}{I_T}$
p	Body fixed nutation rate	0.02509	Hz	$p = \lambda\omega_S$
γ	Wobble Reynold's number	1.5681	none	$\gamma = \frac{pr_{xc}^2}{\nu}$, optimal γ usually ~6
τ	Time constant	31051.6	sec	$\tau = \frac{2\pi I_S}{f(\gamma) r_R^2 M \omega_S (1+\lambda)^2}$
		8.62543	hr	

Chapter 6

Attitude Simulation

A numerical attitude simulation tool is developed for the purpose of analyzing the spinup maneuver. Once developed, this tool also proves useful for hardware simulation and algorithm optimization.

6.1 Simulation Architecture

A top-level flow of this simulation is shown in Figure 6.1.

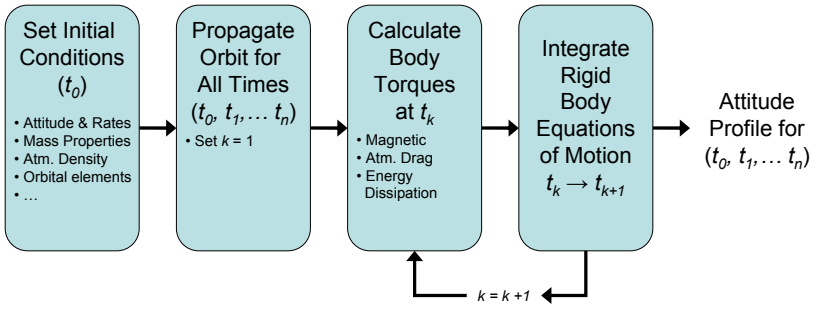

Figure 6.1: Top-level illustration of the flow of information through the attitude simulator.

The simulation begins with a set of user-defined initial conditions on the spacecraft, orbit and environment. It then propagates the orbit forward over the desired length of the simulation, recording the orbit state at every time step. At the first timestep, the instantaneous torques on the spacecraft body from are calculated and

summed. The net force is modeled as an external force acting on a rigid body, and a Runga-Kutta 45 integrator is used to propagate the Euler parameters and angular rates from the current time step to next time step. The instantaneous torques for the new time step are then calculated from the new attitude and orbit state, and these conditions are propagated forward to the next time step. The process continues until the attitude state at each step has been recorded, generating an attitude profile spanning the duration of the simulation.

6.2 Modeling Assumptions

The simulator models the DANDE spacecraft as a system of two rigid bodies consisting of the spacecraft and the fluid within the ring of the nutation damper. Flexible body modes are not considered in the attitude estimation, nor are they expected to be measurable: the DANDE spacecraft is required to have a first fundamental frequency above 100 Hz by the University Nanosat competition rules, which is far faster than any active or disturbance torque frequency expected on orbit.

Certain mass and volume properties are assumed for the DANDE sphere, tabulated in Table 6.1. These are reflective of the mass and volume requirements appearing in the Requirements Flow Down document.

Table 6.1: Assumed physical properties of the DANDE sphere

Property	**Value**
Major Principal Moment (Axial: I_X)	1.14 kg m^2
Minor Principal Moment (Transverse: I_Y, I_Z)	0.99 kg m^2
Mass	50.0 kg
Sphere Radius	0.229 m (9.0 in)

It is assumed that the principle axes of inertial fall exactly on the DANDE primed coordinate axes (see Definition of Attitude section, Figure 6.3). This is done for the sake of simplifying and streamlining the attitude propagation loop. The system requires the

major principal axis to be within 2° of the X direction. The intermediate and minor axes are expected to be very similar in magnitude, so their specific orientation within the plane of ambiguity has minimal influence on the dynamics of the system. For a first-order simulation, the body is assumed to have oblate axisymmetric mass properties about the X' axis.

It is assumed that the orbit and attitude of the spacecraft are decoupled. A first-order orbit propagation routine is used in the code, but only to calculate environmental conditions local to the spacecraft (e.g. atmospheric density, airspeed, local geomagnetic field, etc.)

The modeled external forces on the spacecraft consist of magnetic influences and atmospheric drag. Nutation damper dynamics are not considered external to the system, however their effect on the body frame is shown for scale. As seen in Table 6.2, these are the strongest influences on spacecraft attitude. The modeled effects of the atmospheric drag torque are dominated by the magnetic and nutation damper effects in the spinup simulation. Gravity gradient and solar pressure torques are not modeled because their maximum torque is less than that of the atmospheric drag torque, and since atmospheric drag is shown not to affect the results of the simulation, smaller torques are not expected to alter the results of the simulation either.

6.3 Simulation Description

6.3.1 Orbit Propagation

A number of local environmental variables depend on the instantaneous position and velocity of the spacecraft, which makes it necessary to model the movement of the spacecraft through its orbit. For example, the Earth's magnetic field vector local to the spacecraft depends on its position in the Earth's magnetosphere. Precision orbit modeling and prediction are beyond the scope of this work, but a first-order orbit

Table 6.2: Estimated magnitudes of disturbance torques acting on the DANDE sphere (equations from Space Mission Analysis and Design[7])

Disturbance Torque	Equation for Magnitude	Estimated Torque	Comment
Magnetic Field	$\tau_m = DB$ D = spacecraft magnetic dipole = 5 A·m^2 B = Earth's magnetic field local to spacecraft = 2.58×10^{-5} T	1.3×10^{-4} n·m	Dipole generated by active control of magnetictorque rods. Magnetic field strength at 350 km.
Nutation Damper	$\tau_d = k_d \omega_{w/b}$ k_d = damping constant = 0.001 $\omega_{w/b}$ = rate of fluid bulk moving relative to container walls	1.2×10^{-4} n·m	Assumes 8° half-cone of nutation at 10 RPM. k_d tuned to match required 15 hr time constant.
Atmospheric Drag	$\tau_a = \frac{1}{2}\left(\rho C_d A_V V^2\right)(c_{pa} - cg)$ ρ = local atmospheric density = 1.50×10^{-11} kg/m^3 C_d = coefficient of drag = 2 A_V = cross sectional surface area in ram direction = 0.164 m^2 V = spacecraft velocity = 7697 m/s $c_p - cg$ = distance from aerodynamic center of pressure to center of gravity = 0.01 m	1.5×10^{-6} n·m	Assumes predicted atmospheric activity at 350 km during solar max.
Gravity Gradient	$\tau_g = \frac{3\mu}{2R^3}\lvert I_x - I_y\rvert \sin 2\theta$ μ = Earth's gravity constant = 3.986×10^{14} m^3/s^2 R = orbit radius = 6,728,140 m $I_x - I_y$ = largest and smallest spacecraft moments of inertia = 1.14 − 0.99 = .16 kg·m^2 θ = maximum deviation of I_x from nadir or zenith = $\frac{\pi}{2}$ radians	3.1×10^{-7} n·m	Assumes a maximum $I_x - I_y$ of .16 kg·m^2
Solar Pressure	$\tau_{sp} = \frac{F_s}{c} A_s (1+q) \cos i\,(c_{ps} - cg)$ F_s = solar constant = 1,367 W/m^2 c = speed of light = 3.0×10^8 m/s A_s = cross sectional area in direction of the sun = 0.164 m^2 q = reflectance factor = 1 i = angle of incidence to the sun = 0 radians $c_{ps} - cg$ = distance from solar center of pressure to center of gravity = 1 cm	1.5×10^{-8} n·m	Assumes worst-case reflectance $q = 1$ and $c_{ps} - cg$ same as in atmospheric drag calculation.

propagator is used to model the spacecraft orbit to a fidelity necessary simulate the magnetic and other environmental conditions specific to spacecraft location. Orbital equations of motion (adjusted for the J_2 effect and first-order atmospheric drag) from Tapley et. al.[15] are used for the spacecraft orbital position $\boldsymbol{r}$:

$$\ddot{\boldsymbol{r}} = \ddot{\boldsymbol{r}}_{J2} + \ddot{\boldsymbol{r}}_{\text{drag}} \tag{6.1}$$

where $\ddot{\boldsymbol{r}}_{J2}$ and $\ddot{\boldsymbol{r}}_{\text{drag}}$ are the J_2 adjusted gravitational model of the Earth and the acceleration due to atmospheric drag, respectively. These terms are expanded as follows:

$$\ddot{\boldsymbol{r}}_{J2} = -\left(\frac{\mu}{2r^7}\right)\left[2r^4 - 15J_2R_{\text{earth}}^2Z^2 + 3J_2R_{\text{earth}}^2r^2\right]\boldsymbol{r} \tag{6.2}$$

$$\ddot{\boldsymbol{r}}_{\text{drag}} = -\frac{1}{2}C_d\left(\frac{A}{m}\right)\rho_A V_A \boldsymbol{V}_A \tag{6.3}$$

where $\mu = 3.986 \times 10^{14}$ m^3/s^2 is the gravitational parameter of the Earth, r is the magnitude of the spacecraft position vector $\boldsymbol{r}$, $J_2 = .001082$ is the oblateness of the Earth's mass distribution, $R_{\text{earth}} = 6,378,145$ m is the radius of the Earth, $C_d = 2.0$ is the estimated coefficient of drag of the spacecraft, $A = \pi r_{xc}^2 = .1642$ m^2 is the cross-sectional area of the spacecraft, $m = 45$ kg is the spacecraft mass, ρ_A is local atmospheric density, V_A is the magnitude of the airspeed vector $\boldsymbol{V}_A$, and X, Y, and Z are the Cartesian coordinates of the spacecraft (in m) in the ECI frame. ρ_A is approximated only as a function of altitude:

$$\rho_A = \rho_0 \exp\left[\beta\left(r_0 - r\right)\right] \tag{6.4}$$

where $\rho_0 = 4.0 \times 10^{-13}$ kg/m^3 is the density of the atmosphere at a reference radius of $r_0 = 7,298,145$ m and $\beta = 5.0 \times 10^{-6}$ is a simple scaling factor. $\boldsymbol{V}_A$ is approximated by finding the velocity of the spacecraft in the ECI frame and adding the vector accounting for the rotation of the Earth:

$$\boldsymbol{V}_A = \begin{pmatrix} \dot{X} + \dot{\theta}Y \\ \dot{Y} - \dot{\theta}X \\ \dot{Z} \end{pmatrix} \tag{6.5}$$

where $\dot{\theta} = 7.292 \times 10^{-5}$ radians/second is the rate of rotation of the Earth.

The complete differential equations of motion as implemented in the orbit propagation code are:

$$\begin{aligned}
\ddot{X} &= -\left(\frac{\mu}{2r^7}\right)\left[2r^4 - 15J_2R_{\text{earth}}^2Z^2 + 3J_2R_{\text{earth}}^2r^2\right]X - \frac{1}{2}C_d\left(\frac{A}{m}\right)\rho_A V_A\left(\dot{X} + \dot{\theta}Y\right) \\
\ddot{Y} &= -\left(\frac{\mu}{2r^7}\right)\left[2r^4 - 15J_2R_{\text{earth}}^2Z^2 + 3J_2R_{\text{earth}}^2r^2\right]Y - \frac{1}{2}C_d\left(\frac{A}{m}\right)\rho_A V_A\left(\dot{Y} - \dot{\theta}X\right) \\
\ddot{Z} &= -\left(\frac{\mu}{2r^7}\right)\left[2r^4 - 15J_2R_{\text{earth}}^2Z^2 + 3J_2R_{\text{earth}}^2r^2\right]Z - \frac{1}{2}C_d\left(\frac{A}{m}\right)\rho_A V_A\dot{Z}
\end{aligned} \tag{6.6}$$

Orbit propagation is the first block of code to be executed in the simulation. At every user-defined time step, the position and a velocity of the spacecraft are recorded so they may be passed to functions to calculate disturbance torques.

6.3.2 Definition of Attitude

The "attitude" of the spacecraft is defined as relative orientation of the Earth Centered Inertial (ECI) frame to the body-fixed DANDE primed frame (X',Y',Z'). An illustration of these two frames appear in Figures 6.3 and 6.2.

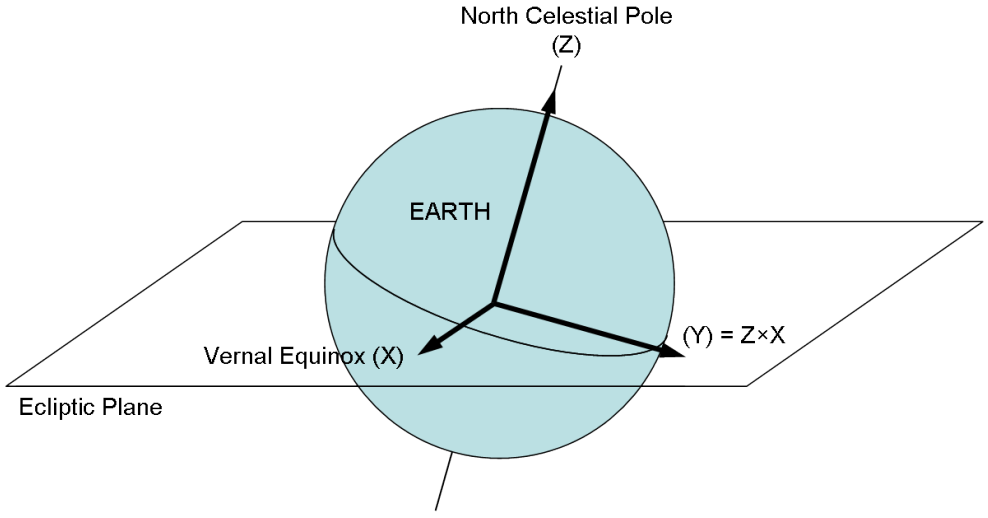

Figure 6.2: Definition of the Earth Centered Inertial coordinate frame.

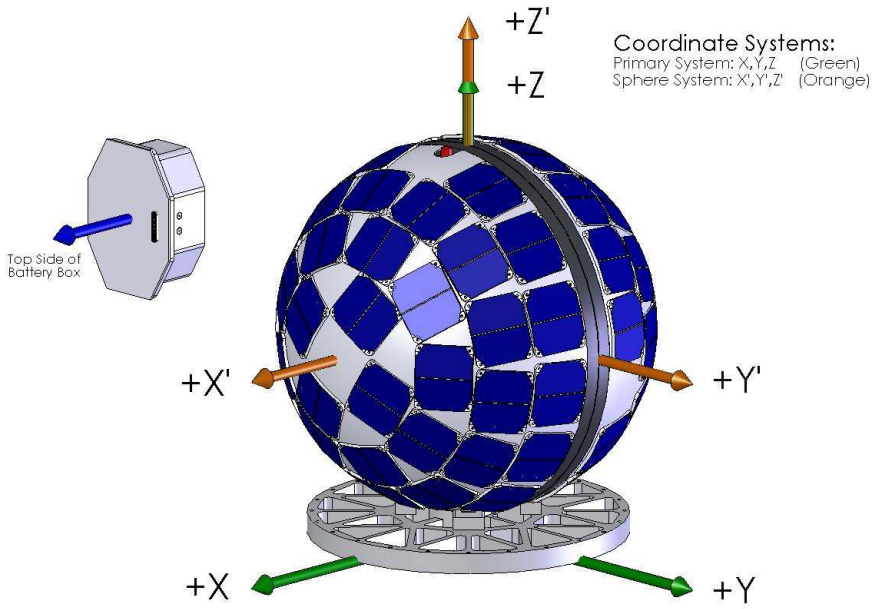

Figure 6.3: Definition of the DANDE body-fixed coordinate frames.

The initial attitude of the spacecraft is input by the user as a transformation from the ECI frame to the body-fixed frame. The transformation from the ECI frame to the body-fixed frame is defined by a 3×3 direction cosine matrix:

$$ {}^{\mathcal{B}}\boldsymbol{b} = \begin{bmatrix} \cos\alpha_{11} & \cos\alpha_{12} & \cos\alpha_{13} \\ \cos\alpha_{21} & \cos\alpha_{22} & \cos\alpha_{23} \\ \cos\alpha_{31} & \cos\alpha_{32} & \cos\alpha_{33} \end{bmatrix} {}^{\mathcal{N}}\boldsymbol{b} = [C]\, {}^{\mathcal{N}}\boldsymbol{b} \tag{6.7} $$

where $\boldsymbol{b}$ is any vector and $\mathcal{N}$ and $\mathcal{B}$ denote the expression of the vector in the ECI frame and body-fixed frame, respectively. The matrix elements $\cos\alpha_{ij}$ represent the dot products of the basis vectors i of the body-fixed frame and the basis vectors j of the inertial frame[11].

It should be noted that the direction cosine matrix (DCM) is only used to input an initial attitude. The DCM carries nine values to define a unique attitude: three of these

values are constrained by unit normality and another three are constrained by the orthogonal property of a rotation matrix. Propagation of the DCM over a long simulation would be needlessly cumbersome. For propagation purposes, the attitude simulation converts the initial attitude to a quaternion (also known as Euler parameters):

$$\boldsymbol{q}_{\mathcal{B}\leftarrow\mathcal{N}} = \begin{pmatrix} q_1 \\ q_2 \\ q_3 \\ q_4 \end{pmatrix} = \begin{pmatrix} e_1 \sin(\Phi/2) \\ e_2 \sin(\Phi/2) \\ e_3 \sin(\Phi/2) \\ \cos(\Phi/2) \end{pmatrix} \tag{6.8}$$

where $\boldsymbol{q}_{\mathcal{B}\leftarrow\mathcal{N}}$ is the quaternion transforming a vector in the $\mathcal{N}$ frame to the $\mathcal{B}$ frame, $\hat{\boldsymbol{e}} = [e_1, e_2, e_3]^T$ is the axis about which the $\mathcal{N}$ frame may be rotated to bring it into alignment with $\mathcal{B}$, and Φ is the angle of rotation to bring the frames into alignment. Note that in Schaub, the Euler parameter are defined as $\boldsymbol{\beta} = [\beta_0, \beta_1, \beta_2, \beta_3]^T$, where the first element β_0 is the scalar component. The Euler parameters may arbitrarily be written either way without loss of functionality.

The conversion from the DCM to Euler parameters using a formula developed by Stanley[14]. The Stanley Method begins by calculating the square of each Euler parameter:

$$\begin{aligned} q_1^2 &= \frac{1}{4}(1 + 2C_{11} - \text{trace}[C]) \\ q_2^2 &= \frac{1}{4}(1 + 2C_{22} - \text{trace}[C]) \\ q_3^2 &= \frac{1}{4}(1 + 2C_{33} - \text{trace}[C]) \\ q_4^2 &= \frac{1}{4}(1 + \text{trace}[C]) \end{aligned} \tag{6.9}$$

The largest q_i^2 is found and the program takes its square root, arbitrarily choosing it to be a positive value. Based on which q_i^2 is the largest, the program finds the other q_i by evaluating the three necessary equations of the following six:

$$
\begin{aligned}
q_4 q_1 &= (C_{23} - C_{32})/4 \\
q_4 q_2 &= (C_{31} - C_{13})/4 \\
q_4 q_3 &= (C_{12} - C_{21})/4 \\
q_2 q_3 &= (C_{23} - C_{32})/4 \\
q_3 q_1 &= (C_{31} - C_{13})/4 \\
q_1 q_2 &= (C_{12} - C_{21})/4
\end{aligned}
\tag{6.10}
$$

At points in the simulation, it becomes necessary to convert the Euler parameters back to a DCM. This is done by the following direct conversion:

$$
[C] = \begin{bmatrix}
q_1^2 - q_2^2 - q_3^2 + q_4^2 & 2(q_1 q_2 + q_3 q_4) & 2(q_1 q_3 - q_2 q_4) \\
2(q_1 q_2 - q_3 q_4) & -q_1^2 + q_2^2 - q_3^2 + q_4^2 & 2(q_2 q_3 + q_1 q_4) \\
2(q_1 q_3 + q_2 q_4) & 2(q_2 q_3 - q_1 q_4) & -q_1^2 - q_2^2 + q_3^2 + q_4^2
\end{bmatrix}
\tag{6.11}
$$

Euler parameters are chosen as the attitude parameter for propagation because of a number of reasons. They carry only four numbers as opposed to the DCM's nine, and they lack the geometric singularities that plague the 3 parameter sets such as the Classical Rodriguez Parameters and the Modified Rodriguez Parameters. Additionally, as will be shown in the Rigid Body Kinematics section, their differential equations are linear, aiding in the speed and accuracy of the state integration.

6.3.3 Single Rigid Body Kinematics and Kinetics

The attitude model was first developed by modeling DANDE as a single rigid body (no nutation damper dynamics). The kinematic equations of motion for the Euler parameters are as follows[11]:

$$
\begin{pmatrix} \dot{q_1} \\ \dot{q_2} \\ \dot{q_3} \\ \dot{q_4} \end{pmatrix} = \begin{bmatrix} 0 & \omega_3 & -\omega_2 & \omega_1 \\ -\omega_3 & 0 & \omega_1 & \omega_2 \\ \omega_2 & -\omega_1 & 0 & \omega_3 \\ -\omega_1 & -\omega_2 & -\omega_3 & 0 \end{bmatrix} \begin{pmatrix} q_1 \\ q_2 \\ q_3 \\ q_4 \end{pmatrix}
\tag{6.12}
$$

where $\boldsymbol{\omega} = [\omega_1, \omega_2, \omega_3]^T$ is the instantaneous rotation vector of the rigid body. If $\boldsymbol{\omega}$ is known as a function of time, the differential equations for the Euler parameters are completely linear. This allows for fast and accurate numerical integration of the equations of motion.

The evolution of $\boldsymbol{\omega}$ is dictated by Euler's rigid body equations of motion[11]:

$$[I]\,\dot{\boldsymbol{\omega}} = -\,[\tilde{\boldsymbol{\omega}}]\,[I]\,\boldsymbol{\omega} + \boldsymbol{L} \tag{6.13}$$

where $[I]$ is the 3×3 moment of inertia tensor taken in the DANDE body frame, $\boldsymbol{L}$ is the net external torque acting on the spacecraft body, and $[\tilde{\boldsymbol{\omega}}]$ is defined as:

$$[\tilde{\boldsymbol{\omega}}] = \begin{bmatrix} 0 & -\omega_3 & \omega_2 \\ \omega_3 & 0 & -\omega_1 \\ -\omega_2 & \omega_1 & 0 \end{bmatrix} \tag{6.14}$$

In the code, the assumption is made that the principal moment axes align with the body-frame coordinate system. The moment of inertia tensor becomes a purely diagonal matrix and the equations of motion can then be simplified to:

$$\begin{aligned} I_{11}\dot{\omega}_1 &= -\,(I_{33} - I_{22})\,\omega_2\omega_3 + L_1 \\ I_{22}\dot{\omega}_2 &= -\,(I_{11} - I_{33})\,\omega_3\omega_1 + L_2 \\ I_{33}\dot{\omega}_3 &= -\,(I_{22} - I_{11})\,\omega_1\omega_2 + L_3 \end{aligned} \tag{6.15}$$

where I_{ii} is the moment of inertia of the body about the i^{th} axis and $\boldsymbol{L} = [L_1, L_2, L_3]^T$ is the net external torque on the system. Note that $\boldsymbol{\omega}$ and $\boldsymbol{L}$ are written in body-frame coordinates, and $[I]$ is formulated with respect to the same frame.

The four Euler parameters and the three angular rates are considered states of the system. A simple Runga-Kutta 45 integrator is used to integrate the state of the system forward in time. A series of states are produced at user-defined intervals for the duration of the simulation. The instantaneous net torque on the body $\boldsymbol{L}$ is updated at every timestep. $\boldsymbol{L}$ is determined by summing the contributions of magnetic field

interactions $\boldsymbol{\tau}_m$ and atmospheric drag torques $\boldsymbol{\tau}_A$:

$$\boldsymbol{L} = \boldsymbol{\tau}_m + \boldsymbol{\tau}_A \tag{6.16}$$

The calculations of the components $\boldsymbol{\tau}_m$ and $\boldsymbol{\tau}_A$ are performed independently and detailed in Sections 6.3.5 and 6.3.6. Note that the nutation damper dynamics are not strictly an external torque, and the equations of motion must be modified to reflect that. This is explained in the following section.

6.3.4 Two-Body Kinematics and Kinetics

The nutation damper is a passive device intended to dissipate kinetic energy from the spacecraft, decaying a random tumble into a minimum-energy, pure spin about the major principal axis. The damper is a fluid-filled ring mounted with the central axis fixed parallel to the Z axis (see Figure 6.4). A pure spin about the X axis creates a centripetal force that is purely normal to the ring. However, if the spacecraft spins about an axis skewed from the major principal axis, Euler's rigid body kinematics dictate that the spin axis will migrate in a cone about the principal axis. This behavior is referred to as "nutation," and causes periodic angular accelerations about any axes perpendicular to the major principal axis.

Since the ring is fixed to the Z axis, the walls of the ring accelerate about the central ring axis sinusoidally whenever there is nutation in the system. This imparts an angular acceleration on the fluid within the ring as viscous forces act to bring the fluid angular velocity to the same rate as the spacecraft. However, this is a non-conservative force, and a portion of the energy used to accelerate the fluid is dissipated as heat. The damper always resists angular acceleration of the ring about its central axis, and the energy dissipation causes the sinusoidal accelerations to exponentially decay over time.

To model the effects of the nutation damper on the spacecraft body, it is assumed that the fluid bulk moves uniformly. This assumption allows the damper to be modeled

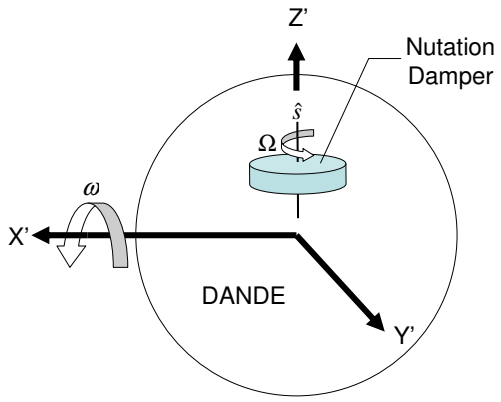

Figure 6.4: The fluid-filled ring nutation damper modeled as a wheel attached to the DANDE frame.

as a rigid body, which can be envisioned as a wheel on an axle fixed to the Z axis, illustrated in Figure 6.4. Since the "wheel" has one degree of freedom, the wheel rate of spin adds an additional state to the system. This state will be termed Ω and will be defined as the angular rate of the wheel relative to the body.

Implementing the dynamics of the nutation damper in the simulation code requires a more intrusive solution than the other modeled torques. This passive "two rigid body system" of a wheel within a body is essentially a reaction wheel that exchanges angular momentum with the spacecraft body. The equation of motion for the wheel is derived by Schaub[11], starting with the general equation for torque on a variable-speed control moment gyroscope (VSCMG). The equation of motion for a VSCMG appears as Equation (4.111) in Analytical Mechanics of Space Systems:

$$\begin{aligned}[I]\,\dot{\boldsymbol{\omega}} = -\boldsymbol{\omega} \times [I]\,\boldsymbol{\omega} - \hat{\boldsymbol{g}}_s \left(J_s \left(\dot{\Omega} + \dot{\gamma}\omega_t \right) - \left(J_t - J_g \right) \omega_t \dot{\gamma} \right) \\ - \hat{\boldsymbol{g}}_t \left(J_s \left(\omega_s + \Omega \right) \dot{\gamma} - \left(J_t + J_g \right) \omega_s \dot{\gamma} + J_s \Omega \omega_g \right) \\ - \hat{\boldsymbol{g}}_g \left(J_g \ddot{\gamma} - J_s \Omega \omega_t \right) + \boldsymbol{L}\end{aligned} \tag{6.17}$$

where $\{\hat{\boldsymbol{g}}_s, \hat{\boldsymbol{g}}_t, \hat{\boldsymbol{g}}_g\}$ are the basis vectors of the CMG frame, aligned with the spin, transverse and gimbal axes respectively, and γ is the angle of the gimbal to the spacecraft

frame. $[J]$ is the moment of inertia matrix of the wheel and gimbal, here written in the gimbal frame: $\{J_s, J_t, J_g\}$. In the case of a reaction wheel there is no gimbal, i.e. the wheel axle is fixed to the frame, thus $\dot{\gamma} = 0$. Immediately the equation simplifies to:

$$[I]\,\dot{\boldsymbol{\omega}} = -\boldsymbol{\omega} \times [I]\,\boldsymbol{\omega} - \hat{\boldsymbol{g}}_s J_s \dot{\Omega} - J_s \Omega \left(\omega_g \hat{\boldsymbol{g}}_t - \omega_t \hat{\boldsymbol{g}}_g\right) + \boldsymbol{L} \tag{6.18}$$

and using the definition of the cross product:

$$[I]\,\dot{\boldsymbol{\omega}} = -\boldsymbol{\omega} \times [I]\,\boldsymbol{\omega} - \hat{\boldsymbol{g}}_s J_s \dot{\Omega} - \boldsymbol{\omega} \times J_s \Omega \hat{\boldsymbol{g}}_s + \boldsymbol{L} \tag{6.19}$$

At this point, the angular momentum of the wheel is broken down by axial and transverse components. In the axial direction, the angular momentum exchange (or torque) u_s on the wheel is defined by Schaub Eq. (4.112):

$$u_s = J_s \left(\dot{\Omega} + \hat{\boldsymbol{g}}_s^T \dot{\boldsymbol{\omega}}\right) \tag{6.20}$$

The momentum of the spinning wheel in only in the $\hat{\boldsymbol{s}}$ direction, therefore there is no momentum exchange between the spacecraft and the wheel in the transverse directions. However, the transverse inertias of the wheel must be accounted for in the $[I]$ matrix of the spacecraft. This modified inertia matrix of the spacecraft with the transverse reaction wheel inertias is termed $[I_{\mathrm{RW}}]$:

$$[I] = \left[I_{\mathrm{S/C}}\right] + [J] \tag{6.21}$$

$$= \left[I_{\mathrm{S/C}}\right] + J_s \hat{\boldsymbol{g}}_s \hat{\boldsymbol{g}}_s^T + J_t \hat{\boldsymbol{g}}_t \hat{\boldsymbol{g}}_t^T + J_g \hat{\boldsymbol{g}}_g \hat{\boldsymbol{g}}_g^T \tag{6.22}$$

$$= [I_{\mathrm{RW}}] + J_s \hat{\boldsymbol{g}}_s \hat{\boldsymbol{g}}_s^T \tag{6.23}$$

Plugging into Eq. (6.19):

$$\left([I_{\mathrm{RW}}] + J_s\hat{\boldsymbol{g}}_s\hat{\boldsymbol{g}}_s^T\right)\dot{\boldsymbol{\omega}} = -\boldsymbol{\omega}\times\left([I_{\mathrm{RW}}] + J_s\hat{\boldsymbol{g}}_s\hat{\boldsymbol{g}}_s^T\right)\boldsymbol{\omega} - \hat{\boldsymbol{g}}_s J_s\dot{\Omega} - \boldsymbol{\omega}\times J_s\Omega\hat{\boldsymbol{g}}_s + \boldsymbol{L}$$

$$[I_{\mathrm{RW}}]\,\dot{\boldsymbol{\omega}} + J_s\hat{\boldsymbol{g}}_s\hat{\boldsymbol{g}}_s^T\dot{\boldsymbol{\omega}} = -\boldsymbol{\omega}\times\left([I_{\mathrm{RW}}]\,\boldsymbol{\omega} + J_s\hat{\boldsymbol{g}}_s\hat{\boldsymbol{g}}_s^T\boldsymbol{\omega}\right) - \hat{\boldsymbol{g}}_s J_s\dot{\Omega} - \boldsymbol{\omega}\times J_s\Omega\hat{\boldsymbol{g}}_s + \boldsymbol{L}$$

$$[I_{\mathrm{RW}}]\,\dot{\boldsymbol{\omega}} + J_s\hat{\boldsymbol{g}}_s\dot{\omega}_s = -\boldsymbol{\omega}\times\left([I_{\mathrm{RW}}]\,\boldsymbol{\omega} + J_s\hat{\boldsymbol{g}}_s\omega_s\right) - \hat{\boldsymbol{g}}_s J_s\dot{\Omega} - \boldsymbol{\omega}\times J_s\Omega\hat{\boldsymbol{g}}_s + \boldsymbol{L}$$

$$[I_{\mathrm{RW}}]\,\dot{\boldsymbol{\omega}} = -\boldsymbol{\omega}\times\left([I_{\mathrm{RW}}]\,\boldsymbol{\omega} + J_s\hat{\boldsymbol{g}}_s\omega_s\right) - J_s\hat{\boldsymbol{g}}_s\dot{\omega}_s - \hat{\boldsymbol{g}}_s J_s\dot{\Omega} - \boldsymbol{\omega}\times J_s\Omega\hat{\boldsymbol{g}}_s + \boldsymbol{L}$$

$$[I_{\mathrm{RW}}]\,\dot{\boldsymbol{\omega}} = -\boldsymbol{\omega}\times[I_{\mathrm{RW}}]\,\boldsymbol{\omega} - \boldsymbol{\omega}\times J_s\omega_s\hat{\boldsymbol{g}}_s - J_s\left(\dot{\omega}_s + \dot{\Omega}\right)\hat{\boldsymbol{g}}_s - \boldsymbol{\omega}\times J_s\Omega\hat{\boldsymbol{g}}_s + \boldsymbol{L}$$

Working out the cross products by components:

$$\boldsymbol{\omega}\times J_s\omega_s\hat{\boldsymbol{g}}_s = -\omega_t J_s\omega_s\hat{\boldsymbol{g}}_g + \omega_g J_s\omega_s\hat{\boldsymbol{g}}_t$$

$$\boldsymbol{\omega}\times J_s\Omega\hat{\boldsymbol{g}}_s = -\omega_t J_s\Omega\hat{\boldsymbol{g}}_g + \omega_g J_s\Omega\hat{\boldsymbol{g}}_t$$

and continuing to simplify:

$$\begin{aligned}[I_{\mathrm{RW}}]\,\dot{\boldsymbol{\omega}} = -\boldsymbol{\omega}\times[I_{\mathrm{RW}}]\,\boldsymbol{\omega} &- J_s\omega_s\left(\omega_t\hat{\boldsymbol{g}}_g - \omega_g\hat{\boldsymbol{g}}_t\right)\\ &- J_s\Omega\left(\omega_t\hat{\boldsymbol{g}}_g - \omega_g\hat{\boldsymbol{g}}_t\right)\\ &- J_s\left(\dot{\omega}_s + \dot{\Omega}\right)\hat{\boldsymbol{g}}_s\end{aligned}$$

Recombining components into cross products:

$$J_s\omega_s\left(\omega_t\hat{\boldsymbol{g}}_g - \omega_g\hat{\boldsymbol{g}}_t\right) = \boldsymbol{\omega}\times J_s\omega_s\hat{\boldsymbol{g}}_s$$

$$J_s\Omega\left(\omega_t\hat{\boldsymbol{g}}_g - \omega_g\hat{\boldsymbol{g}}_t\right) = \boldsymbol{\omega}\times J_s\Omega\hat{\boldsymbol{g}}_s$$

and realizing:

$$J_s\left(\dot{\omega}_s + \dot{\Omega}\right) = J_s\left(\dot{\boldsymbol{\Omega}} + \hat{\boldsymbol{g}}_s^T\dot{\boldsymbol{\omega}}\right) = u_s$$

we arrive at the final equation of motion for spacecraft portion of the two body system:

$$[I_{\mathrm{RW}}]\,\dot{\boldsymbol{\omega}} = -\boldsymbol{\omega}\times[I_{\mathrm{RW}}]\,\boldsymbol{\omega} - \boldsymbol{\omega}\times J_s\left(\omega_s + \Omega\right)\hat{\boldsymbol{g}}_s - u_s\hat{\boldsymbol{g}}_s + \boldsymbol{L} \tag{6.24}$$

This solution matches Eq. (4.113) in Schaub and Junkins.

To be used in the simulator, u_s must be written in terms of states or inputs to the system. The axial torque on the nutation damper wheel from the body is assumed to be directly proportional to Ω:

$$\boldsymbol{\tau}_D = u_s \hat{\boldsymbol{s}} = k_w \Omega \hat{\boldsymbol{s}} \tag{6.25}$$

where k_w is a constant defined by the properties of the fluid and the housing. As is described in Chapter 5, the nutation damper is designed such that it decays the half-cone of nutation with a time constant of 8.6 hours. The value of k_w is adjusted such that the behavior of the system matches this time constant.

Substituting Eq. (6.25) into the equations of motion for the two body system yields

$$[I_{\mathrm{RW}}]\,\dot{\boldsymbol{\omega}} = -\boldsymbol{\omega} \times [I_{\mathrm{RW}}]\,\boldsymbol{\omega} - \boldsymbol{\omega} \times J_s\,(\omega_s + \Omega)\,\hat{\boldsymbol{g}}_s + k_w \Omega \hat{\boldsymbol{g}}_s + \boldsymbol{L} \tag{6.26}$$

which is how the equations of motion for the spacecraft are integrated in the MATLAB code. The equation of motion for Ω is integrated according to Eq. (6.25) substituted into Eq. (6.20):

$$\dot{\Omega} = \frac{k_w}{J_s} - \hat{\boldsymbol{g}}_s^T \dot{\boldsymbol{\omega}} \tag{6.27}$$

As mentioned before, the torque that the body experiences from the nutation damper u_s is an internal torque. Therefore, in a torque-free environment, the total angular momentum vector of the spacecraft plus the nutation damper must be conserved. This constant of motion provides a convenient check for the fidelity of the model. Under a randomly selected set of initial conditions and a torque-free environment, the angular momentum vector of the spacecraft body and the angular momentum vector of the wheel sum to a constant total vector over the duration of the simulation, verifying the model.

A second check is performed using kinetic energy. Under random initial conditions in a torque-free environment, the kinetic energy of the body frame will exponentially decay to a pure spin about the major principal axis and the kinetic energy of the wheel

will eventually decay to zero. The simulation satisfies this second check and the attitude model is accepted as verified.

6.3.5 Magnetic Torque Modeling

A body exhibiting a magnetic dipole $\boldsymbol{m}$ in the presence of a magnetic field $\boldsymbol{B}$ will experience a magnetic torque $\boldsymbol{\tau}_m$ according to the equation[2]:

$$\boldsymbol{\tau}_m = \boldsymbol{m} \times \boldsymbol{B} \tag{6.28}$$

In the simulation, $\boldsymbol{m}$ is the magnetic dipole created by an active torque rod. DANDE has two torque rods, one aligned with the X axis and one aligned with the Y axis. Either of these torque rods may create a dipole in either direction, or be inactive. The activation of the torque rods is controlled by algorithms specific to the mode of the spacecraft. For example, polarity switching for the spinup algorithm is explained in Chapter 7.

Since the torque rods are rigidly fixed to the body frame, the vector $\boldsymbol{m}$ is easily written using the user-defined maximum magnetic dipole. For example, if the Y axis torque rod were to be activated with maximum dipole strength d_{max} in the positive direction (i.e. the +Y end of the torque rod seeks the Earth's magnetic North pole), DANDE's net magnetic dipole would be $\boldsymbol{m} = [0, d_{max}, 0]^T$.

Obtaining $\boldsymbol{B}$ in the magnetic torque equation is more difficult. To first-order accuracy, the Earth's magnetic field can be modeled as a simple dipole, but the field is constantly drifting and fluctuating in shape. To obtain the highest-possible fidelity model for the Earth's magnetic field during the time span of the mission, a MATLAB program written by Carlos Roithmayr of NASA Langley Research Center is used to generate a high-fidelity geomagnetic model based on the International Geomagnetic Reference Field (IGRF). This program accepts inputs of a Cartesian coordinate in the ECI frame and a Julian date and outputs the Earth's predicted $\boldsymbol{B}$ vector in the ECI

frame at that point in time, as predicted by the IGRF. The function uses up to 10^{th} degree, 10^{th} order spherical harmonics by default, and the Schmidt-normalized coefficients are based on the 1995 IGRF.

At each time step of the attitude propagation, $\boldsymbol{B}$ is found in the ECI frame. The attitude of the spacecraft at that time step is converted to a 3×3 rotation matrix by Eq. 6.11, which is subsequently used to convert $\boldsymbol{B}$ into body-frame components. This ${}^{\mathcal{B}}\boldsymbol{B}$ vector is plugged into Eq. 6.28 to calculate the magnetic torque $\boldsymbol{\tau}_m$.

6.3.6 Atmospheric Drag Modeling

It is assumed that the DANDE geometry is a perfect sphere, i.e. the cross section from any angle is a circle of a constant radius (9 inches). The center of pressure is assumed to be in the center of the circle with a cross section normal to the ram direction (Figure 6.5). The atmospheric drag force on the spacecraft is modeled as a point force in the direction opposing ram at the center of pressure with a magnitude of:

$$F_A = \frac{1}{2} C_d \left(\frac{A}{m} \right) \rho_A V_A^2 \tag{6.29}$$

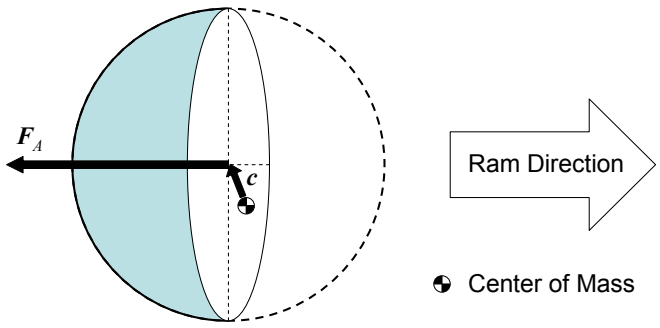

Figure 6.5: Example atmospheric drag free-body diagram.

The torque on the body is calculated as the cross product between the vector

from the center of mass to center of pressure $\boldsymbol{c}$ and $\boldsymbol{F}_A$:

$$\boldsymbol{\tau}_A = \boldsymbol{c} \times \boldsymbol{F}_A \tag{6.30}$$

The vector $\boldsymbol{c}$ is fixed in the body frame. This is a user-defined constant vector, and for the purposes of the worst-case simulation, its magnitude is limited to < 1.0 cm per the mass properties requirements. $\boldsymbol{F}_A$ is found by taking the spacecraft velocity vector in the ECI frame and converting it to the body-fixed frame using the same procedure used to convert $\boldsymbol{B}$ in the Magnetic Torque Modeling section. With $\boldsymbol{c}$ and $\boldsymbol{F}_A$ expressed in the body frame, $\boldsymbol{\tau}_A$ is also expressed in the body frame, allowing it to be plugged directly into Eq. 6.16.

Chapter 7

The Spinup Manuever

To validate the requirements on the spinup maneuver (Table 7.1), a simulation is run in the simulator described in Chapter 6. These requirements drive the sizing of the torque rods and nutation damper, and an error in these requirements could cause design problems to cascade through the whole ADC subsystem.

Table 7.1: These are the requirements to be validated through the Spinup Maneuver Simulation.

Req. Number	Description
2.ADC1	The Attitude Determination and Control (ADC) subsystem shall achieve its final attitude state within 144 hours (six days) of subsystem activation.
3.ADC4	The DANDE spacecraft shall achieve the spin rate magnitude about the X' body axis in a closed loop control mode starting from the following worst-case attitude condition in the nominal orbit: oriented with the Y torque rod perpendicular to the ecliptic and spinning at .1 rad/sec about the body Y-axis.
3.ADC5	The DANDE spacecraft shall achieve its required spin rate within 24 hours of subsystem activation.
4.ADC6.1	The closed loop spin up algorithm will operate by continuously sampling the local magnetic field in the direction of the Y torque rod and switching the polarity of the current as a peak magnitude is reached.
4.ADC6.2	The closed loop spin up algorithm will automatically shut down when the commanded spin rate described in 3.ADC2 is reached.

7.1 Assumptions

The simulation is carried out on the MATLAB model described in the Attitude Simulation section of this thesis. All assumptions made in that model apply to the simulated spinup maneuver.

The spherical shape of the craft forces the torque rods to be contained within the primary structure, meaning that the changing magnetic field will induce currents in the surrounding metallic structure. These are called "eddy currents", which reduce the effective magnetic dipole of the spacecraft. Eddy currents are difficult to model on complex metallic structures, so a conservative margin is used instead. The strength of the magnetic dipole created by the torque rods is modeled to be 5 $A \cdot m^2$. This gives 2 $A \cdot m^2$ of margin under the 7 $A \cdot m^2$ dipole strength required by 4.ADC3.5. The control algorithm used to activate and reverse the polarity of the torque rod is detailed in Section 7.2.

The Design Reference Mission (DRM) orbit is used for this analysis. The DRM is a nominal orbit and mission operations timeline for the DANDE mission. The purpose of the DRM is to instate a reference orbit and timeline for for which subsystems may optimize their design. This is a sun-synchronous, near polar orbit at 350 km. The Keplerian elements used as initial orbit conditions appear in Table 7.2, and a visualization of this orbit appears in Figure 7.1.

As part of DRM operations, during spinup mode the spacecraft will only exercise active control at latitudes between -40° and +40°. As the spacecraft travels over the poles, the torque rods will be inactive. This is the duty cycle used on SNOE to maintain a power-positive maneuver and to actuate through a predictable magnetic field for the alignment maneuver. In the case of DANDE, this is a soft requirement put in place to keep consistency between maneuvers. It is conservative in that it keeps the torque rods off for a greater portion of the duty cycle than called for by the power budget, and may

Table 7.2: Keplerian orbital elements of the Design Reference Mission.

Keplerian Element	Value
Semi-Major Axis	6,728.14 km
Eccentricity	0.00
Inclination	96.86°
Right Ascension of Ascending Node	99.91°
Argument of Periapsis	0.00
True Anaomaly	0.00

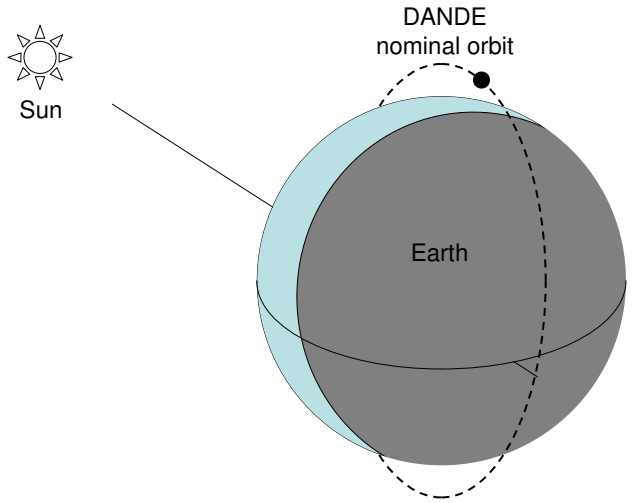

Figure 7.1: Visualization of the design reference mission's 350 km, sun synchronous noon-midnight orbit.

be pushed back if necessary.

The spinup simulation also assumes that the magnetometer and the torque rods may be operated simultaneously. The control law that closes the loop between the sensor and the actuator is based only on the first derivative of the magnetic field. Because the control law uses "bang-bang" control (either a torque rod is on or off), the first derivative of the field created by the torque rod is zero while the rod is in use. If the magnetometer used is capable of measuring the Earth's magnetic field superimposed over the magnetic field created by the torque coils, it should not be necessary to operate the torque rods

and magnetometer in a duty cycle. This will be verified in a bench-level test using the flight-model magnetometer and torque rods in a the shell of DANDE. It should be noted that most missions using a B-dot control law use the magnetic sensors and actuators in a duty cycle.

An upper bound on the rate of initial rotation is also assumed. By assuming the launch vehicle is at rest when the Lightband is triggered, the Lightband performs as indicated in the UN5 User's Guide, and that the DANDE sphere separating from the LAB has no more than three times the tip-off rate of the Lightband, the greatest angular rotation rate expected in the space-sector-sphere is 0.10 radians/second. The initial axis of rotation is unknown.

7.2 Algorithm

The strategy for the spinup algorithm is to add kinetic energy to the system and to allow the nutation damper to decay the tumble into pure spin about the principal axis. The final orientation of the pure spin vector in the ECI frame is not important at this point.

The torque rods are electromagnets, creating a magnetic dipole when a voltage is applied to the electrical contacts. As discussed in the Attitude Simulation chapter, this dipole will experience a torque $\boldsymbol{\tau}$ to align itself with the Earth's magnetic field according to the equation $\boldsymbol{\tau} = \boldsymbol{m} \times \boldsymbol{B}$, where where $\boldsymbol{m}$ is the magnetic moment of the dipole and $\boldsymbol{B}$ is the Earth's magnetic field vector local to the spacecraft. The torque rod creates this dipole by passing a current through a coil of wire wrapped around a ferromagnetic core. The Y torque rod is required by 4.ADC3.3 to be capable of creating at least 7 A·m^2 of magnetic dipole. By adding the aforementioned margin to account for lose due to eddy currents, the total moment exhibited by the system is conservatively modeled at 5 A·m^2.

The control law for the spinup maneuver is based on the B-dot concept. A

visualization of the concept appears in Figure 7.2. Notice the similarity between Figure 7.2 illustrating spin acceleration and Figure 2.1 showing B-dot spin damping: only the direction of the magnetic dipole is reversed.

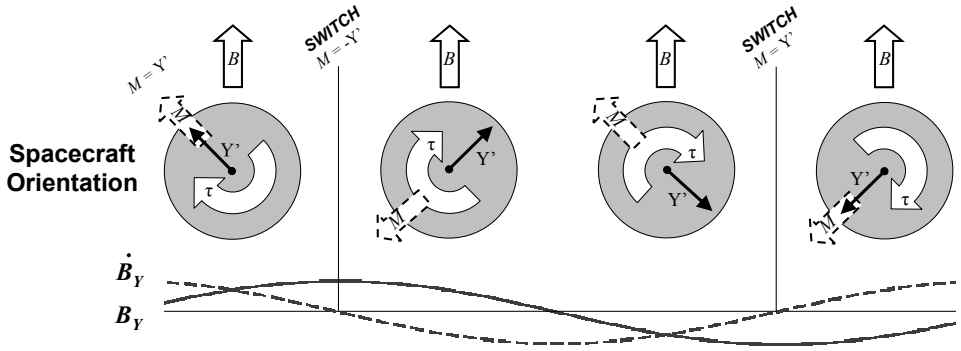

Figure 7.2: The Spinup Control Algorithm concept. As the spacecraft rotates so that the Y axis more closely aligns with the Earth's B-field, the first derivative of the B-field in the Y direction is positive. The Y axis torque rod creates a magnetic dipole in the +Y direction, creating a torque **increasing** the spin rate. The dipole direction is reversed when the Y axis passes the B-field direction and $\dot{B}_Y$ becomes negative.

To create rotation about the X' axis (positive or negative; the spacecraft functionality is insensitive to the difference), only the Y axis torque rod is utilized. Since the torque created by $\boldsymbol{m} \times \boldsymbol{B}$ is perpendicular to both $\boldsymbol{m}$ and $\boldsymbol{B}$, it would be impossible to use the X torque rod to generate torque about the X' axis.

The algorithm begins by collecting and logging a short history magnetic field data in the direction of the Y torque rod (B_y). The derivative of that history is then found numerically ($\dot{B}_y$). Because the local B-field in the ECI frame is assumed to be nearly constant over a one second interval, if the derivative is positive, the spacecraft must be rotating such that the Y torque rod is becoming more closely aligned with the B-field. Activating the Y torque rod in this case will torque the spacecraft to accelerate this rotation, which is the desired effect. Therefore, if the derivative of the component of the B-field in the Y torque rod direction is positive, the Y torque rod is activated.

If the derivative of the B-field in the Y torque rod direction is negative, it suggests

that the spacecraft is rotating such that the Y torque rod is becoming less aligned with the local B-field. Activating the torque rod in this case would decelerate the rotation, which is the undesired effect. However, a negative derivative also means that the vector in the opposite direction of the Y torque rod is rotating to become closer aligned with the local field. A dipole in the opposite direction can be created simply by reversing the current through the electromagnet. Like in the original case, this accelerates the already existing spin. This "switching" algorithm continuously pumps kinetic energy into the system until the spacecraft is spinning at 10 RPM about its X'-axis.

A block diagram of the baseline spinup algorithm is shown in Figure 7.3.

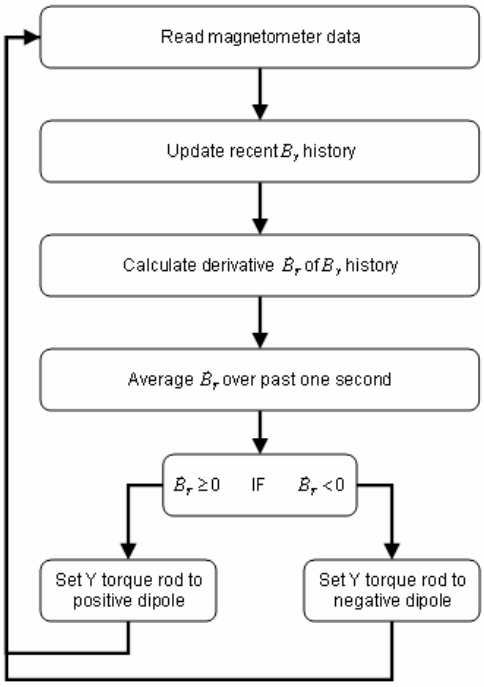

Figure 7.3: Flow diagram of the baseline spinup algorithm.

In the simulation, the data used is perfect, so a single pair of data points would be sufficient to find the derivative of the field at that point. On orbit, the data will be taken by a magnetometer that will report a signal with some white noise associated with it. This requires the system to implement either a digital or analog filtering scheme. To

de-couple the filtering issue from the algorithm, a time delay is used on a true signal. The one-second time average used here is to simulate the delay in the magnetometer signal from collection through filtering or post-processing and creation of a useful first derivative signal. A one-second average provides an upper bound on the data post-processing lag time.

In the simulation, the magnetometer data is sampled in 100 ms intervals and one second of data is retained, resulting in 10 data points in the log. The derivative of the function is numerically calculated between each point, resulting in 9 derivative data points. These points are averaged to determine whether the magnitude is increasing or decreasing.

7.3 Approach

The attitude state of the spacecraft is unknown at the beginning of the mission. This includes the orientation of the spacecraft in the ECI frame, the rate of rotation, the direction of rotation, and the true anomaly at which the algorithm will be activated. The location of the spacecraft center of mass is also unknown within the bounds of the requirements, so it is also placed at a random location. To address these unknowns, a Monte Carlo simulation is performed with each of the unknowns randomized over reasonable bounds:

- Initial orientation is randomized by selecting four random elements of a quaternion between zero and one, then normalizing the quaternion to unity.
- Initial rotation rate is randomized by selecting a rate between zero and 0.1 rad/sec, the upper bound on rate found by the tip-off analysis.
- Initial rotation direction in the body frame is randomized by the combination of an azimuth (uniformly distributed zero to 2π radians) and elevation (sinusoidally distributed between $-\pi$ and π radians.)

- Starting true anomaly is randomized between zero and 2π radians.
- The vector from the geometric center of the spacecraft to the center of mass is a vector with direction normalized by the same process used to select the rotation direction, and magnitude randomized between zero and 1.0 cm.

Using the baseline control algorithm, 100 random initial condition test cases are run and the attitude state at every time step recorded. The time between steps is set to 0.1 in order to keep the attitude-dependent torques (magnetic, atmospheric drag) current even at the fastest anticipated rates of rotation. The time required to attain $\pm$ 10 RPM for each of these cases is recorded and presented in the following section. To limit the amount of simulation time, test cases are terminated at 30 hours if they have not achieved the required spin rate by then.

7.4 Results and Discussion

The progression of the spacecraft's attitude state is monitored by plotting the components of the spin axis vector in the body frame over time. A typical example of this plot appears in Figure 7.4.

In this example, the DANDE space sector sphere attained the required 10 RPM spin rate in 6.4 hours, well under the 24 hour requirement. Note that the flat sections of the ω_X curve occur as the spacecraft passes above +40° and below -40° latitude, where active control is not used.

The results from the 100 combined tests are shown in Figure 7.5.

According to the data shown in Figure 7.5, the majority of the initial conditions simulated easily meet the 24 hour spinup requirement. Of the 100 cases tested, only ten failed the requirement, a 90% success rate. From this test suite, it can be inferred that when DANDE initiates the spinup maneuver, it is likely that the baseline spinup algorithm will bring the spacecraft to its final attitude state within the required time.

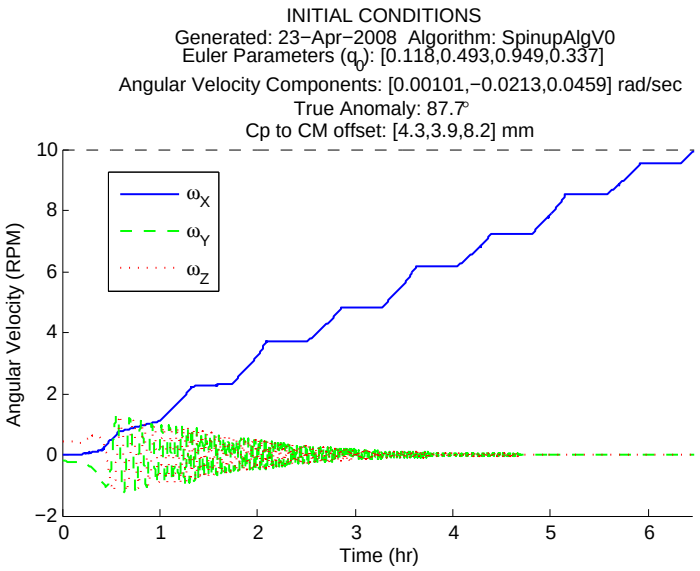

Figure 7.4: Example of typical spinup behavior.

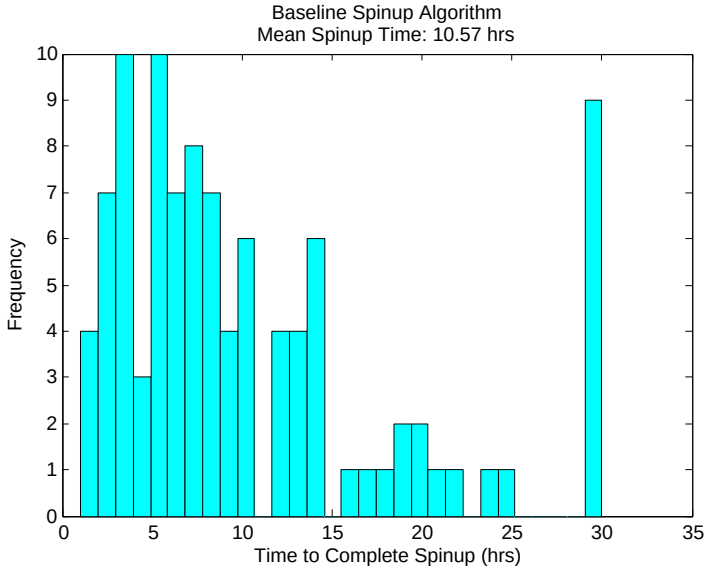

Figure 7.5: Distribution of times to complete spinup maneuver using the baseline algorithm. Note that all cases exceeding 30 hours are truncated at 30, therefore the displayed mean is not the true mean of all spinup times.

However, it can also be seen that it is possible for DANDE to begin the spinup maneuver

in such an attitude state that very long spinup times will result from the baseline algorithm. These long-spinup cases constitute worst-case initial conditions and must be mitigated.

7.5 Mitigation Strategy

A watchdog program is proposed as a risk mitigation strategy. The program monitors data from the magnetometer and watches for initial conditions indicative of a possible long-spinup attitude state. If these conditions are found, then the watchdog temporarily overrides the spinup algorithm and sends a pre-determined sequence of commands to the torque rods to move the sphere out of the long-spinup attitude state.

7.5.1 First Generation: "mit2"

A first-generation mitigation algorithm dubbed 'mit2' is developed and implemented. mit2 simulates a watchdog that detects a long-spinup attitude state by monitoring the periodic frequency of the magnetometer data. If the frequency of the data does not increase by a threshold quantity in five hours, the watchdog halts the spinup algorithm and takes control of the torque rods. For the following 90 minutes, the X axis torque rod is activated in the positive direction in the actuation latitudes, then the normal spinup control law is reapplied. A block diagram demonstrating this logic appears in Figure 7.6.

When implemented on the initial conditions leading to long spinups under the baseline algorithm, the mit2 logic is shows little difference in the results and fails to bring any of the non-compliance cases under 30 hours. The angular rates of one of these cases is shown in Figure 7.7. Not only does mit2 fail to improve the total spinup time noticably, it hardly has any effect on the rates of the spacecraft at all. This suggests that in the long spinup cases, DANDE is in an orientation where neither torque rod has good torque authority over the spacecraft. The focus in optimizing the algorithms is

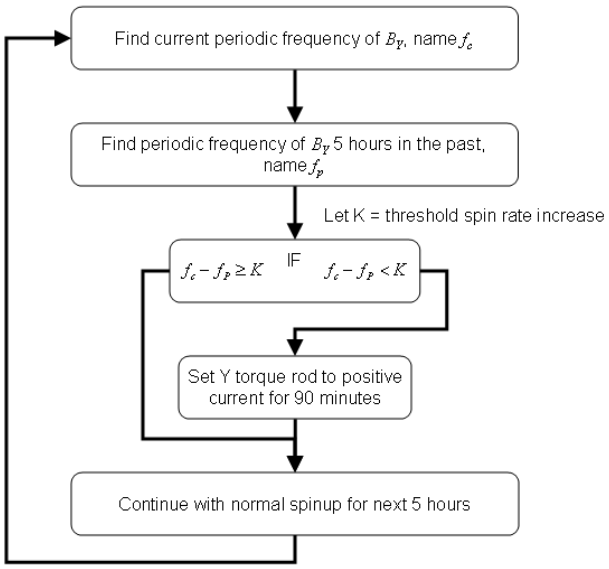

Figure 7.6: Flow chart showing the control logic of 'mit2'.

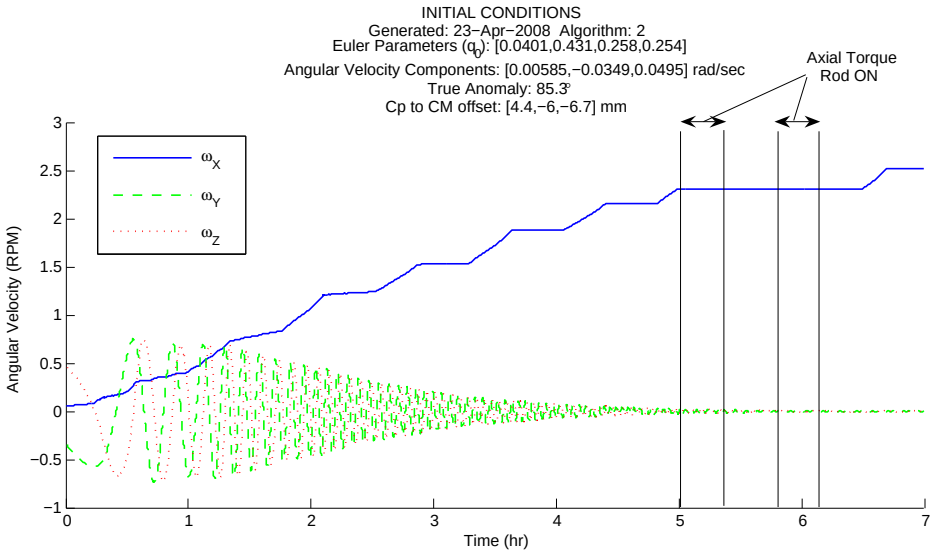

Figure 7.7: First six hours of a long spinup case with mit2 control logic implemented. Note that statically activating the axial torque rods at the indicated points has little effect on the rotation of the spacecraft.

shifted to preventing these unfavorable conditions early in the maneuver.

7.5.2 Second Generation: "mit3"

It is hypothesized that the energy missing from the long spinup cases may be going into rotations about the transverse basis vectors Y and Z. To mitigate this risk, an algorithm is developed to actively damp out rotations about the Y and Z directions. This is the usual application of the B-dot control law as used on FalconSAT-3 and others.

It is proposed to improve mit2 by using a de-spinning algorithm about the Y axis (similar to the FalconSAT-3 B-dot law) instead of a static activation of a torque rod. The de-spinning algorithm is similar in concept to the unmitigated spinup algorithm, but damping out a spin instead of amplifying it. The X torque rod is be switched to negative polarity if the B-field in the X direction is increasing, and visa versa (see Figure 2.1 in the Literature Review section). This algorithm is intended to slow the current spin instead of accelerating it, and could be a more controlled method of putting the spacecraft in a favorable spinup attitude state.

To prevent the ADC subsystem from exceeding the power budget, the spin and de-spin torques are put on a duty cycle. The timing of the algorithm is also adjusted to match the orbit period. The baseline spinup algorithm is implemented for two orbits, then the damping algorithm is implemented for the next orbit, and the process repeats. The flow of this control law is shown in Figure 7.10.

This iteration of the mitigation strategy is named "mit3" and implemented on all of the non-compliant cases of the unmitigated spinup simulation. Figures 7.8 and 7.9 compare the effect of the baseline and mit3 algorithms on the same set of unfavorable initial conditions. All non-compliant cases under the baseline algorithm respond similarly to the mit3 algorithm.

As seen in the example case in Figures 7.8 and 7.9, mit3 performs worse than the baseline strategy. The two strategies behave very similarly in the sections where they

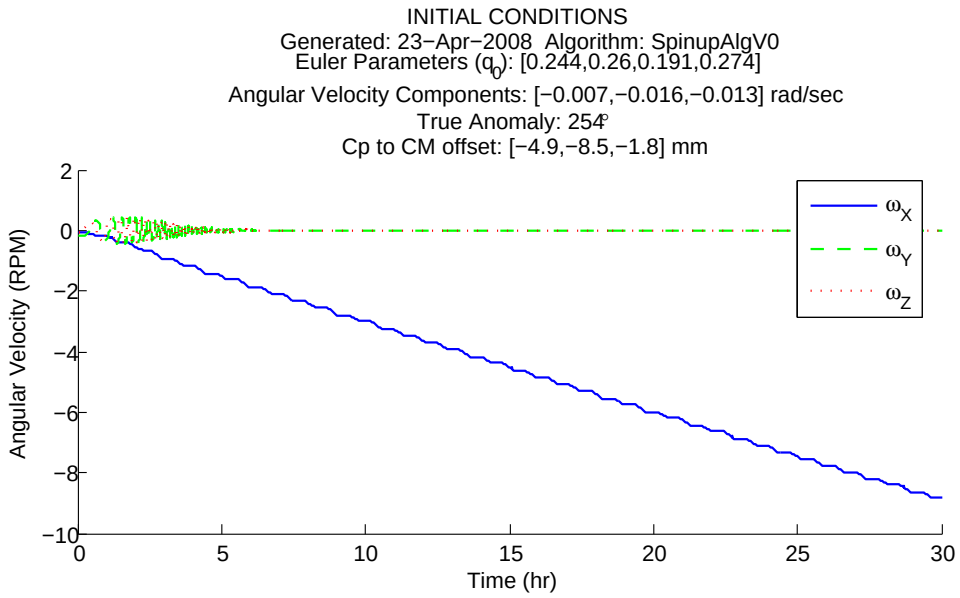

Figure 7.8: Example of long spinup under the baseline algorithm.

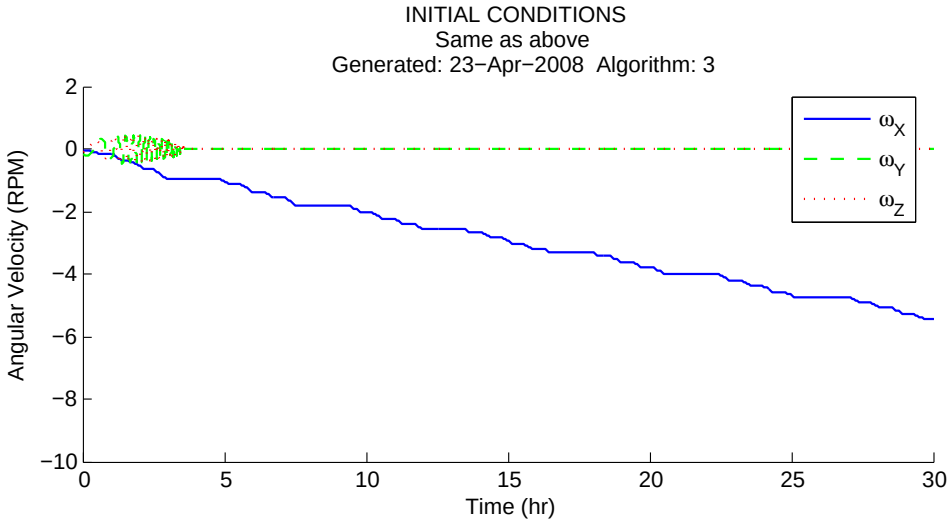

Figure 7.9: Same long spinup under the mit3 algorithm.

use the B-dot control law to accelerate about the X axis, but the overall performance of mit3 is degraded by the pauses in the acceleration maneuver to actively damp nutation. As shown in Figure 7.9, the active damping is extremely effective early in the maneuver,

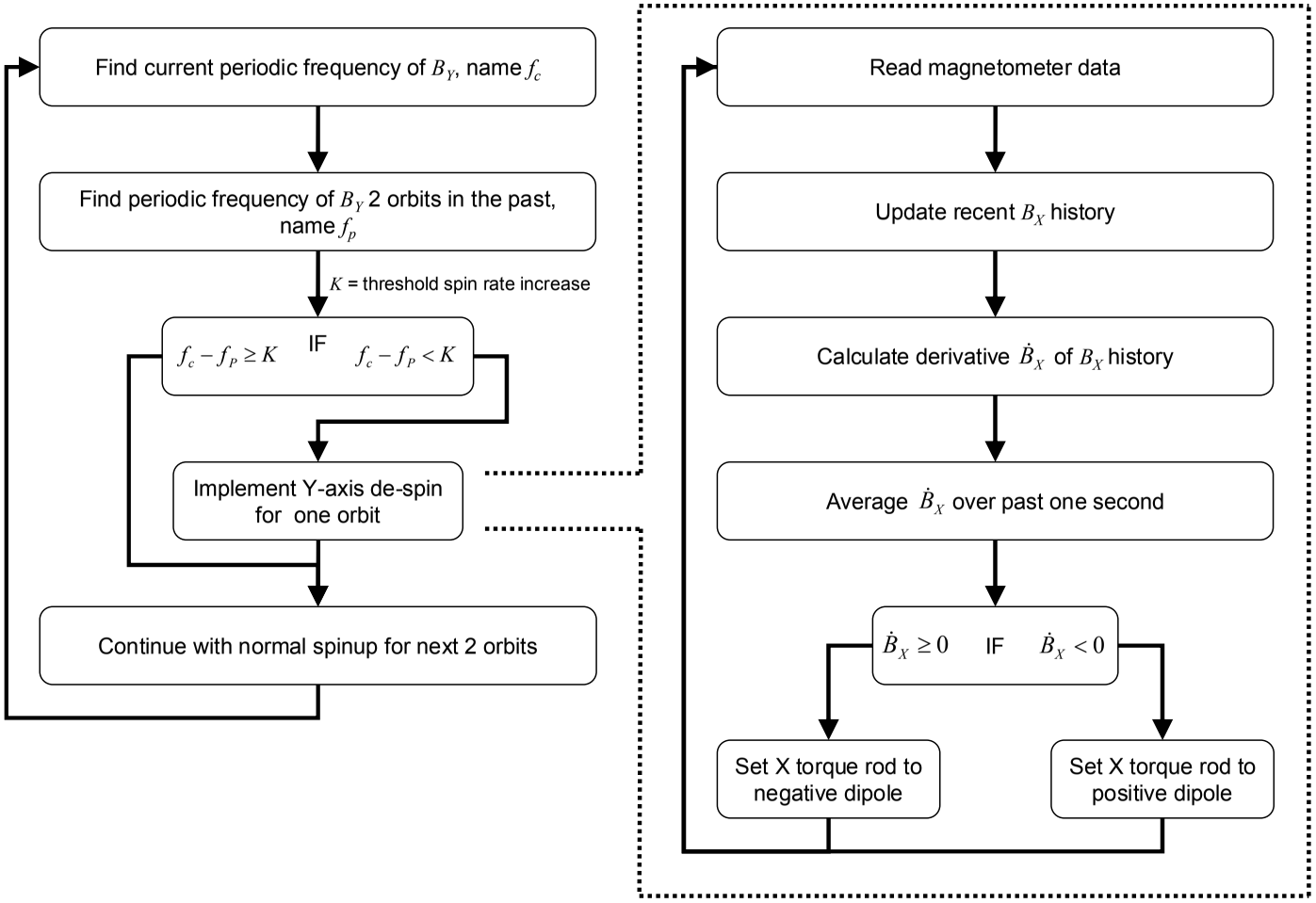

Figure 7.10: Flow chart showing the control logic of 'mit3'.

but is not necessary after a few hours. This is wasted time that the algorithm could be using to accelerate the spacecraft. This mitigation strategy is deemed ineffective and the focus is again shifted to determining the cause of the reduced authority of the torque rods in the long spinup cases.

7.5.3 Third Generation: "mit6"

After several variants of mit2 & mit3 were explored in mit4 & mit5 without success or new insight, a new strategy is proposed. It is hypothesized that the DANDE sphere looses authority to spin up in cases where it develops angular momentum in a vector closely aligned to the Earth's magnetic field. Since the actuation of DANDE occurs only at equatorial latitudes, the orientation of the magnetic field in the ECI frame does not vary much over the distance that DANDE actuates. Should DANDE be put into a major-axis pure spin about this vector, neither torque rod provides an effective torque out of that orientation: the axial rod is closely aligned to $\boldsymbol{B}$, so the magnitude of $\boldsymbol{m} \times \boldsymbol{B}$ is small, and the transverse torque rod creates a torque nearly orthogonal to the direction of the spin axis, making it ineffective in accelerating the spin.

It is proposed to "swap" the duty cycle of the active and inactive phases. In mit6, if a bad spinup condition is detected in the first two orbits, the spacecraft switches to actuating over the poles and coasting between latitudes of $\pm 50^{\circ}$ latitude. By this strategy, the actuation duty cycle is preserved and thus there is no impact on the power budget. In addition, instead of being forced to re-orient the spacecraft out of a bad alignment to the B-field, because the magnetic field reverses polarity in an orbit over the Earth's poles, the B-field is guaranteed to move out of an unfavorable orientation to the spacecraft at least twice per orbit. Finally, the density of magnetic field lines is increased near the poles, providing more torque on the spacecraft for the same magnetic moment generated.

A comparison of the baseline algorithm to mit6 for the same initial conditions seen in the mit3 discussion is shown in Figures 7.11 and 7.12.

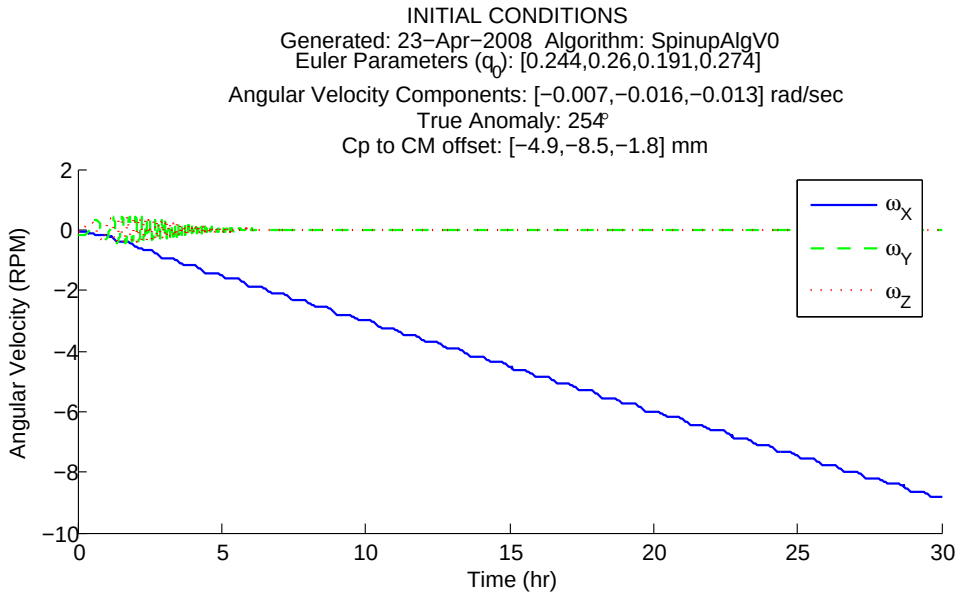

Figure 7.11: Example of long spinup under the baseline algorithm.

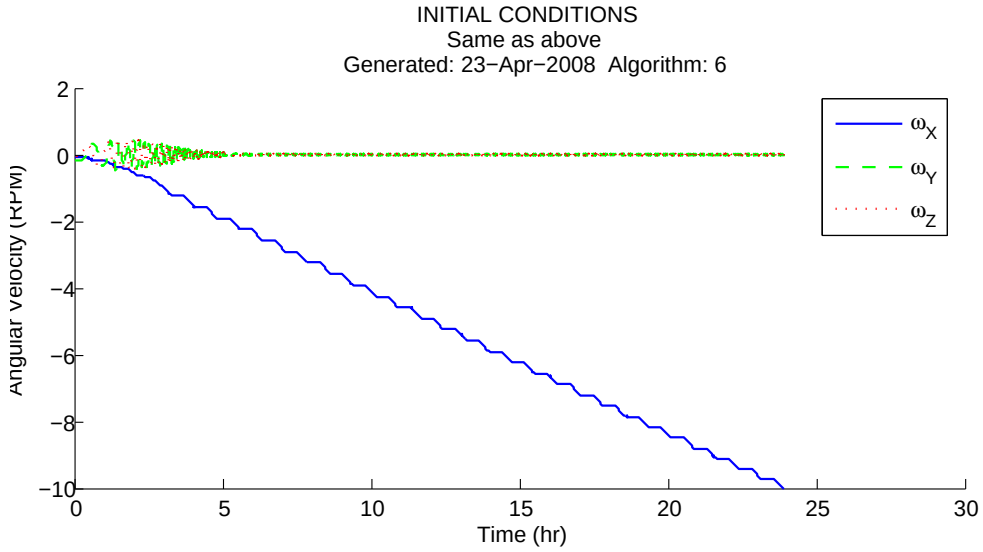

Figure 7.12: Same long spinup under the mit6 algorithm.

The mit6 algorithm clearly outperforms the baseline algorithm. The slope of the ω_X line is steeper than that of the baseline algorithm, suggesting that the new strategy puts DANDE in a position to have greater authority over the magnetic torques on the system. All other long spinup cases showed similar improvement, however only one case was brought back within the spinup requirement.

It is proposed that all initial condition cases could be improved by actuating over the poles instead of the equator. Instead of using a watchdog program, the duty cycle could be swapped for the duration of the spinup maneuver. A similar Monte Carlo was carried out to test this hypothesis, the results of which appear in Figure 7.13. Comparing this figure to Figure 7.5, some improvement over the baseline performance is seen. The method of actuating over the poles and recharging the batteries over the equator meets the spinup requirement in 95 out of 100 tested cases. However, to complete the worst-case analysis, there is still work to be done to find mitigation techniques for the final

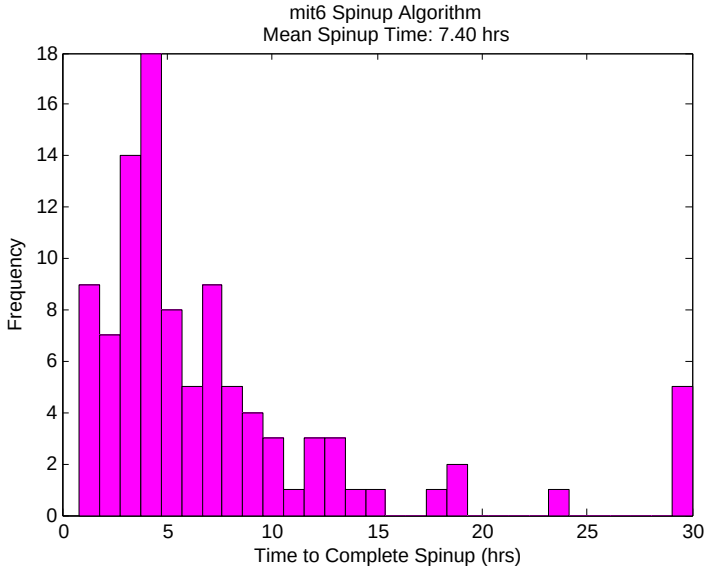

Figure 7.13: Distribution of times to complete spinup maneuver using the mit6 algorithm from the start of spinup. Note that all cases exceeding 30 hours are truncated at 30, therefore the displayed mean is not the true mean of all spinup times.

5% of slow spinup conditions.

7.5.4 Future Algorithm Improvement

The root cause of unfavorable spinup conditions still remains unknown. An interesting study would be to investigate the correlation between the initial angular momentum direction and the time needed to spin up. The hypothesis proposed in the mit6 discussion should be tested. If true, there may be a more efficient way of detecting a bad orientation early in the maneuver and smartly avoiding generating angular momentum about an unfavorable vector.

A watchdog program to detect unfavorable spinup conditions may still prove useful in mitigating the final 5% of long spinup cases. However, to date there has been no development work on this program, and it should be modeled and tested before proposed as a viable option. Although not demonstrated here, it seems possible that the mitigation algorithm could alter a good initial attitude state into a long-spinup state if the watchdog triggers on the wrong case. Once better developed, the watchdog trigger and mitigation algorithm should be tested on the entire suite of initial conditions tested here.

This algorithm also depends on the assumption that the magnetometer and torque rods may be used concurrently. There is a serious risk that this may not be the case, pending results of a bench-level test. Heritage would strongly suggest that the algorithm be modified to operate sensors and actuators on a duty cycle.

7.6 Conclusion

Using the baseline spinup algorithm, the DANDE sphere will attain its design spin rate of 10 RPM in less than 24 hours for approximately 90% of expected initial conditions. This can be improved to 95% by actuating over the polar regions instead of the equator. This mitigation can be implemented using existing hardware and one

additional software program. Further investigation into the cause of unfavorable spinup conditions is required to further optimize the spinup algorithm.

Chapter 8

Worst-Case Attitude Determination Analysis

A study is conducted to ensure that the Horizon Crossing Indicators and baseline determination algorithm provide adequate information to meet the attitude determination requirements under a worst-case attitude and orbit. The requirements validated by this study are shown in Table 8.1.

8.1 Determination Architecture Background

To perform attitude determination, DANDE utilizes Horizon Crossing Indicators (HCIs) per requirement 3.ADC12. An HCI is an optical instrument which signals a change in the luminescence of its field of view. The field of view of the instrument is typically very small, around a 3° full-cone. Radiation enters the instrument and passes through a filter, then hits a pyroelectric detector which generates a voltage proportional to the time rate of change of illumination.

Carbon dioxide emits infrared radiation at a wavelength near 15 microns. By tuning the filter to this frequency, the HCI can be used to detect the presence of carbon dioxide in its field of view. Carbon dioxide resides in a relatively thin layer of the atmosphere against the surface of the Earth, so the HCI becomes an Earth sensor. If the HCI is mounted to a spacecraft spinning about a vector $\boldsymbol{\omega}$, it will trace out a circle on the celestial sphere of the spacecraft as seen in Figure 8.1.

At the point where the sensor boresight crosses from the sky to Earth or Earth

Table 8.1: These are the requirements to be validated through the Attitude Determination Worst-Case Analysis.

Req. Number	Description
2.ADC3	The ADC subsystem shall determine the attitude of DANDE with respect to the velocity or cross-track directions to within 2° during density measurement cycles.
3.ADC8	Determination of the spin axis orientation during science collection shall determine the spin axis to a 1° half-angle cone around the true axis orientation with an updated state(s) at least once every 12 hours.
3.ADC9	Determination of the spin vector magnitude shall determination the spin rate to within ±0.5 degree per second at least once every 12 hours.
3.ADC14	During initial alignment and re-alignment phases, the spin axis shall be determined to a 4° half-cone around the true axis orientation. Goal: meet determination requirements of 3.ADC8 during alignment phase.
4.ADC5.1	During science collection, the ADC subsystem will collect and pass to the ground sector no less than ten consecutive sky-Earth intervals (time in sky, time in Earth) of HCI data at no less than five points in the orbit separated by a change in true anomaly of no less than 40°. Goal: 90% of all crossing intervals of most recent complete orbit.
4.ADC5.2	While operating in alignment mode, the ADC subsystem will collect and pass to the ground sector no less than ten consecutive sky-Earth intervals (time in sky, time in Earth) of Horizon Crossing Indicator data at no less than five points in the orbit separated by a change in true anomaly of no less than 40°. Goal: 90% of all crossing intervals of most recent complete orbit.
4.ADC5.3	Attitude determination while the spacecraft is at or near its design spin rate will be performed using deterministic two-cone intersection techniques using the user-defined best two points of data described in 4.ADC5.1. Goal: batch processor to statistically determine best state estimate.
4.ADC5.4	The ground sector shall recognize erroneous crossings from sun or moon sightings and remove this data from true crossing data described in 4.ADC5.1

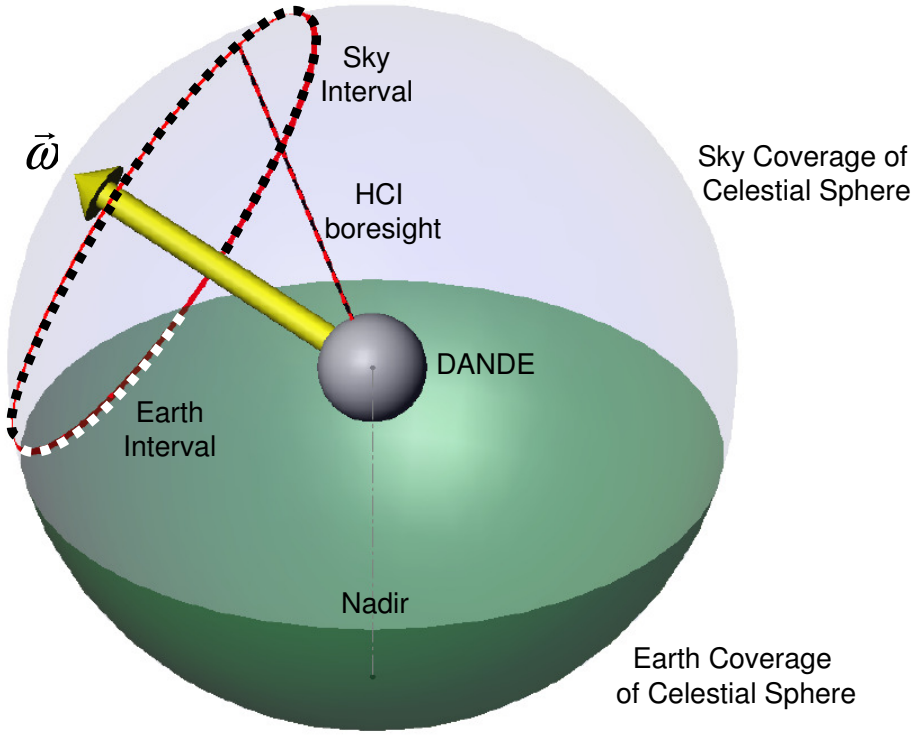

Figure 8.1: Example trace of the path of an HCI on DANDE's celestial sphere. The black dotted line indicates where the HCI points at the sky and the white dotted line indicates where the HCI points at the Earth.

to sky, the detector sees a rapid change in illumination, causing a voltage spike. The time of the spike is recorded and logged by the Command and Data Handling (CDH) computer. By taking a rotation of data and looking at the relative time the HCI points at the sky vs. the Earth, the angle between $\boldsymbol{\omega}$ and nadir can be determined (further detail is provided in the Approach section). For the terms of this analysis, this value will be termed "roll."

If the position of the spacecraft is known at more than one point in the orbit, this data can be combined with roll angle at both points to determine the direction of in inertial 3-space.

This architecture has extensive flight heritage among orbit-normal spinning spacecraft, including SNOE.

8.2 Assumptions

Three-axis determination is only required once the spacecraft has achieved its required X-axis spin rate of 10 RPM for science data collection. Before this state has been reached, only the alignment of the spacecraft relative to the local magnetic field is necessary to perform spinup. Therefore it is assumed that the spacecraft will have a positive or negative rotation about the body X axis of 10 RPM when the HCIs are in use.

It is also assumed that the spacecraft is exhibiting a pure spin about the principal moment. This assumption is based on 4ADC4.1, which requires the nutation damper to decay the rotation of the system to a pure spin about the principal moment with a time constant of less than 15 hours. Following 24 hours of spinup (required by 3.ADC5), the half-cone nutation envelope of the spacecraft will have decayed to about 10% of its original amplitude, which simulations show to average around 10°. Under these conditions, the most nutation the spacecraft could undergo at the point where determination is required is a 1° half-cone. Each ground pass is roughly 12 hours apart, so after the second

ground pass the nutation envelope will be less that half a degree. 2.MTS10 requires knowledge of the principal axis alignment to less than half a degree, and 3.STR1.24 requires the alignment of the sensors to less than one degree. With these tight knowledge requirements, the uncertainty in the angle of the sensors is assumed to be zero. Known deviations in alignment from nominal do not significantly affect the performance of the system within the bounds named in 4.ADC1.1 and 2.MTS7.

It is also assumed that the spin axis of the spacecraft remains fixed in inertial space over the course of 1/9th of an orbit. This is verified in later simulations. Requirements on the determination algorithm are for spacecraft modes that will not use active attitude control, and disturbance torques are projected to be low. The spherically shaped spacecraft is ideal for the rejection of atmospheric drag torques and solar radiation torques. Gravity gradient torques are also small due to the confined volume of the DANDE sphere, and with the mass trim requirements on the system, will only act as restoring forces about the nominal attitude. The spacecraft will also be rotating at no less than 10 RPM about its major axis, and the angular momentum of the system will further desensitize the spacecraft to these small disturbance torques.

The response of the HCI to the spacecraft environment is simulated as an independent function. The model is developed with the help of the vendor and closely emulates the projected performance of the actual sensor, as described in the Results section. Sensor noise is included in this simulation, as described in Section 8.4. It is assumed, however, that the input to the sensor is "perfect": the Earth is modeled as a sphere (no equatorial oblateness), the radiance from the atmosphere varies linearly and uniformly from 20 km to 50 km of altitude, and there are no erroneous sources of illumination such as the sun and moon.

The round Earth assumption is adequate due to the low altitude of the mission: at 350 km, the geometric difference between a round and the oblate Earth model is less than half a degree difference from nadir to the horizon at the worst point. The linear

gradient of radiance in the atmosphere is based on Figure 3 of "Sensing Accuracy of a Conical Scan C02 Horizon Sensor" by R. Weiss[17]. The erroneous illumination filtering is required by 4.ADC5.4. Since determination will be done by the ground sector in this open-loop scheme, the operator will be able to look at the collected data and remove sections that they deem to be erroneous (or the process could be automated through a variety of filtering methods.) This applies not only to false positives, but also to false negatives and attitude states where the HCI does not cross the horizon.

Two HCIs are assumed to be mounted with their fields of view at 45° to the equatorial plate as seen in Figure 8.2. This is the same configuration as the SNOE mission.

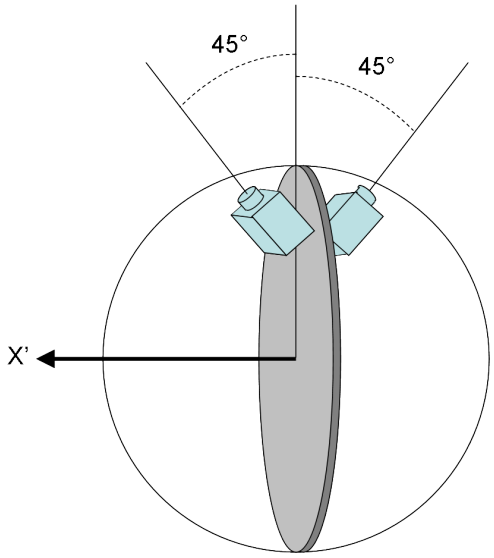

Figure 8.2: Mounting configuration of horizon crossing indicators.

The worst-case attitude for determination occurs when the orbit and attitude initial conditions are such that the resulting attitude state through the orbit produces the minimum amount of usable data from the HCIs. This is determined to be the case if, at any one point in the orbit, the spin axis is pointed directly at nadir, as illustrated in 8.3

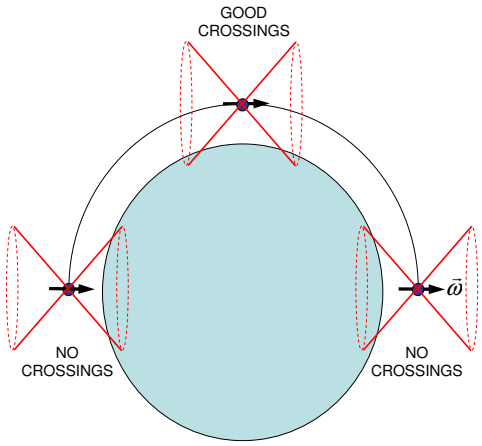

Figure 8.3: Illustration of the worst-case spin axis direction for attitude determination.

In a nadir-pointing spin, one HCI traces out a circle on the Earth and the other traces out a circle in the sky. Neither instrument crosses the horizon, so no useful data is collected at this point in the orbit. One-quarter orbit later, the spin vector is pointed tangent to the orbit and the HCIs collect good data. One-quarter orbit after tangent, the spin axis points to zenith and no crossings are seen again. This orientation of the spin axis provides the smallest range of the orbit in which good crossing data can be obtained, therefore it is considered the worst-case orbit.

8.3 Algorithm

The baseline attitude determination algorithm operates in two phases: roll determination at a single point in the orbit, and combining roll data from two different points on the orbit to produce the spin axis direction in 3-space.

At any given point in an orbit, the data collected by the HCIs may determine the spin rate about the X axis and the "roll" angle, which we define to be the angle between the spin axis and nadir, illustrated in Figure 8.4.

Determining roll angle is not enough information to fully determine the orientation of the spin axis. There is an ambiguity about the nadir axis, and the set of possible

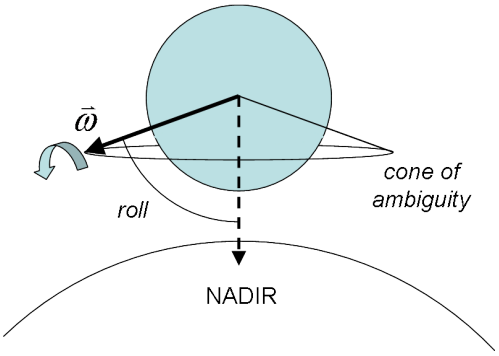

Figure 8.4: Definition of the "roll" angle for the DANDE mission.

spin vectors trace out a cone about this direction. In order to determine the true spin vector in 3-space, the roll angle must be measured at a second point in the orbit. Since the spin axis is assumed to remain stationary in the ECI frame, the detected roll angle will change as the spacecraft moves around the Earth, illustrated in Figure 8.5.

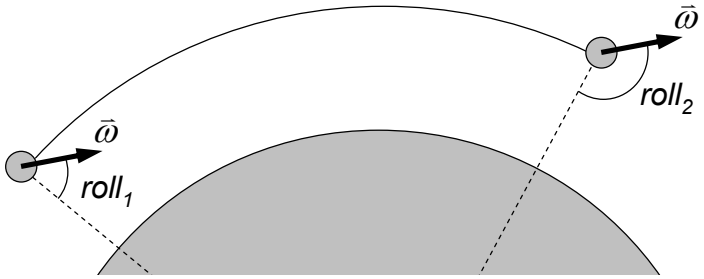

Figure 8.5: Illustration of how roll angle changes along the orbit as $\boldsymbol{\omega}$ remains constant.

By measuring the roll angle at two different orbit positions, two cones are created in inertial space, both containing the spin axis vector $\boldsymbol{\omega}$. The spin axis vector is found by solving for the intersection of two cones, illustrated in Figure 8.6.

As seen in Figure 8.6, the intersection of two cones has two solutions in most cases. One solution will be $\boldsymbol{\omega}$, the other will be the reflection of $\boldsymbol{\omega}$ about the plane formed by the centerlines of the two cones. Since both cones are about nadir vectors at different points on the orbit, this is also the orbit plane. This final ambiguity can be

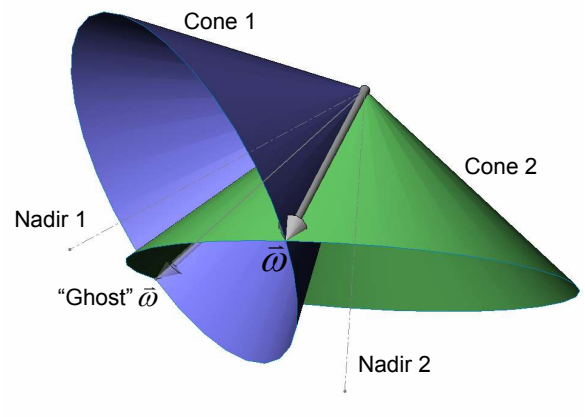

Figure 8.6: How a single $\boldsymbol{\omega}$ is resolved from two different cones of ambiguity.

resolved by use of the magnetometer. While the magnetometer cannot provide precision attitude measurements at a high rate of spin, it can provide enough data to determine which of the two vectors cannot be the true $\boldsymbol{\omega}$. Also, this ambiguity need be resolved only once, and the movement of the true $\boldsymbol{\omega}$ can be tracked forward without confusing it with the "ghost" vector opposite it in the orbit plane.

8.4 Simulation Approach

The determination simulation is decomposed into six separate blocks of code, as shown in Figure 8.7.

One orbit of attitude data in the case described in Section 8.2 is generated in the Spacecraft Attitude Simulation block. This is considered to be the "true" attitude state over the course of the simulation. This data is input to the HCI Field of View Calculator function, which finds the energy seen by the HCI based on the its angle to nadir. This function incorporates both the finite thickness of the horizon and the field of view of the instrument.

The time function of irradiance on the detector is input into the HCI Sensor Simulator module. This block reported perceived crossing times as would be read by the HCI

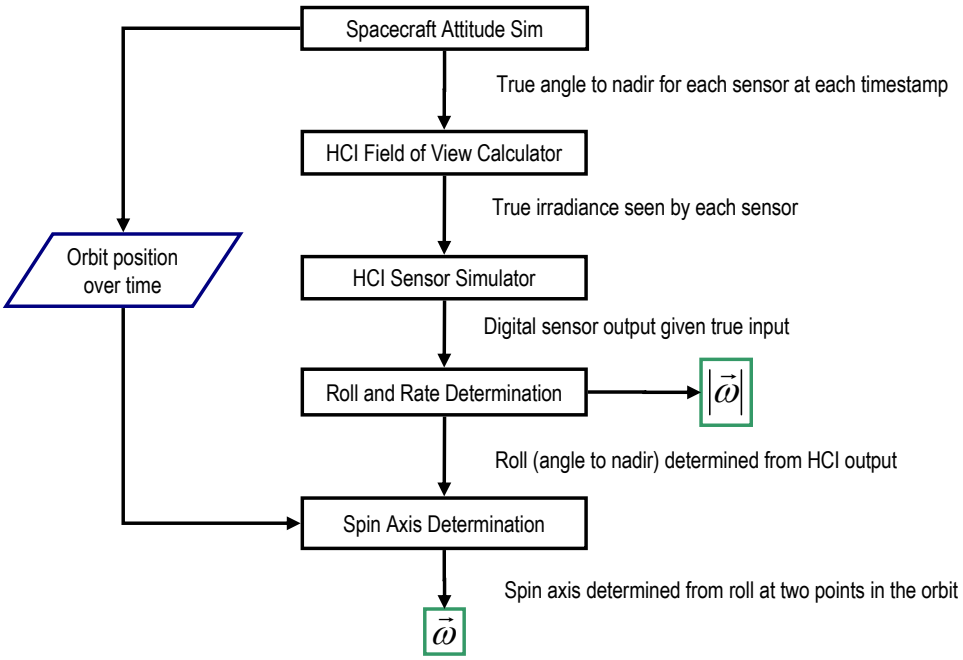

Figure 8.7: Flow chart of the attitude determination simulation.

with important sensor dynamics simulated. These included the rise time of the pyroelectric detector, white noise on the detector circuit, digital sampling and quantization, and trigger threshold values. The output of this function is a list of two consecutive time intervals that each HCI spent looking at the Earth of sky between indicated crossings. The magnitude of the spin rate is extracted from this data.

The two intervals of data are averaged and the resulting average intervals are passed into the roll determination function. This function converts the time intervals to path lengths on the celestial sphere, as shown in Figure 8.8.

In Figure 8.8, roll angle is defined to be η. γ is the angle between the spin axis and the HCI boresight, which is known *a priori* by direct measurement prior to launch. ρ is the angle from nadir to the horizon as seen by the spacecraft, which is a function only of the spacecraft's current altitude and is determined independently of attitude. Ω is the angle traced out by the Earth interval of the HCI path.

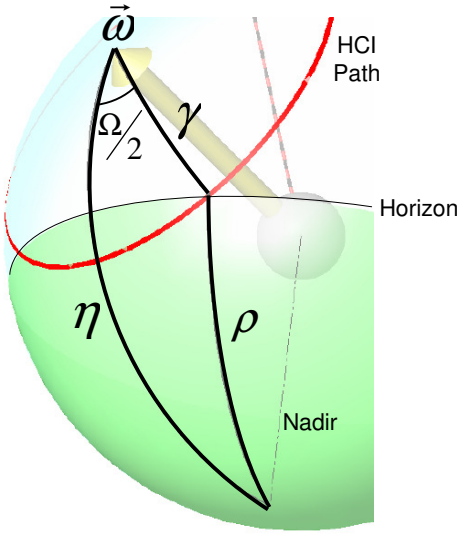

Figure 8.8: Illustration of the spherical angles used in calculating roll angle.

On the sphere in Figure 8.8, these three angles form sides of a spherical triangle. γ and ρ are known before determination is preformed. To find the roll angle η, at least one internal angle of the spherical triangle must be known. This information is provided by the HCIs. The Earth interval divided by the sky plus Earth interval gives the fraction of a full circle occupied by the Earth interval. This angle is defined to be Ω. Because the Earth is assumed to be a perfect sphere, $\Omega/2$ forms the internal angle between η and γ. Using spherical trigonometry, η can be found by the relation

$$\tan(\eta) = \frac{-\cos(\gamma) + \sqrt{\cos^2(\gamma) + \sin^2(\gamma)\cos^2\left(\frac{\Omega}{2}\right) - \cos^2(\rho)}}{\sin(\gamma r)\cos\left(\frac{\Omega}{2}\right) + \cos(\rho)} \tag{8.1}$$

Roll angle η is generated at two points in the same orbit with a separation of 40° of true anomaly. These roll angles and nadir vectors are fed into the Spin Axis Determination block, which calculates the intersection of the two cones as seen in Figure 8.6. The ghost spin axis is assumed to be eliminated, and the resulting $\boldsymbol{\omega}$ is compared to the true spin vector generated in the first block of code. At this point a judgment can be made as to whether the determination scheme met the requirements.

The process is repeated several thousand times with the same initial conditions and the distribution of the output is analyzed to determine how the white noise within the HCI causes the determined spin axis to fall outside the determination requirements.

8.5 Results and Discussion

Referring to Figure 8.7, first the true angle to nadir is generated for the HCI at 10 RPM at a given point on orbit using the Spacecraft Attitude Simulation block. Results are shown in Figure 8.9.

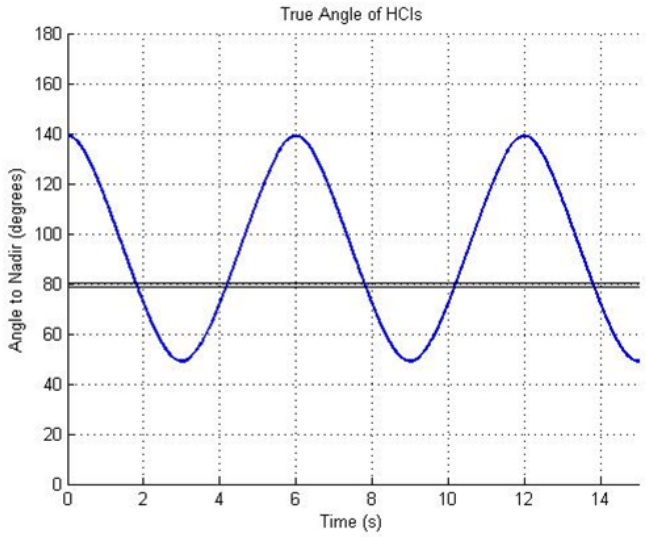

Figure 8.9: True angle from HCI boresight to nadir as the spacecraft spins at 10 RPM.

The double black line near 80° in Figure 8.9 delineates the angle from nadir to the horizon. Below that angle, the HCI sees only the Earth and above that angle the HCI sees only sky. The line is double to indicate that the horizon is not a knife-edge, but has some transition range where the temperature at a point on the celestial sphere would be somewhere in between the Earth temperature and sky temperature.

Using the true angle, data is converted to true energy into the HCI aperture in the HCI Field of View Calculator block. Results are shown in Figure 8.10.

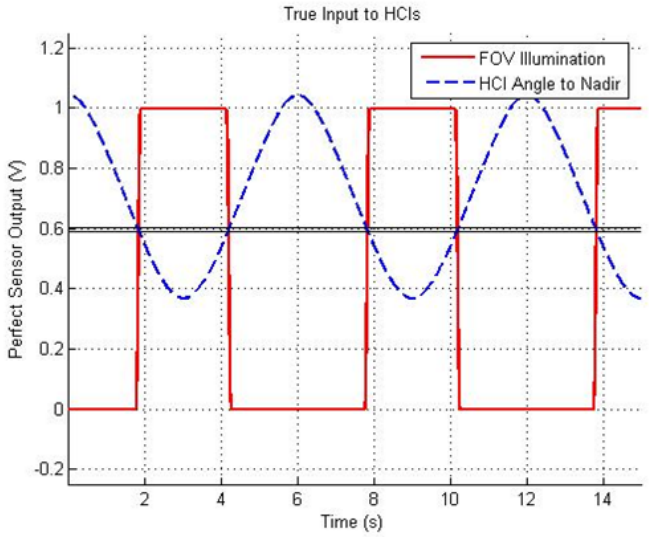

Figure 8.10: True energy incident on HCI detector (normalized to unity) overlayed on the true angle to nadir.

As expected, the energy is high when the HCI points at the Earth and low when the HCI points at the sky. However, notice that the field of view (FOV) illumination is not a perfect square wave. Due to the finite thickness of the atmosphere and the 3° field of view of the instrument, each transition has a finite slope and rounded corners.

The FOV true illumination data is fed into the HCI Sensor Simulator block. This code simulates the dynamics of the sensor hardware (specifically the detector and RC circuit), adds white noise to the detected signal, and returns a digital output signal based on when a crossing is detected. Results are shown in Figure 8.10.

To check the fidelity of the simulation, this sensor simulation is compared against sample data collected by the vendor, seen in Figure 8.12. Comparing Figures 8.11 and 8.12, it can be seen that the simulation dynamics match very closely with the observed data. It can also be seen that the white noise simulated in Figure 8.11 is safely conservative over the noise seen in the vendor generated data.

The HCI Sensor Simulation block converts voltages above the threshold values into timestamps indicating a horizon crossing and the direction of the crossing (Earth-

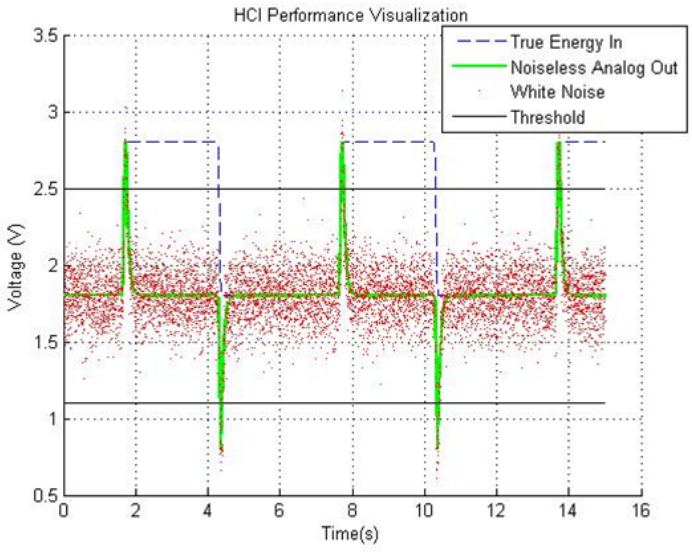

Figure 8.11: HCI performance as produced by the numerical simulation.

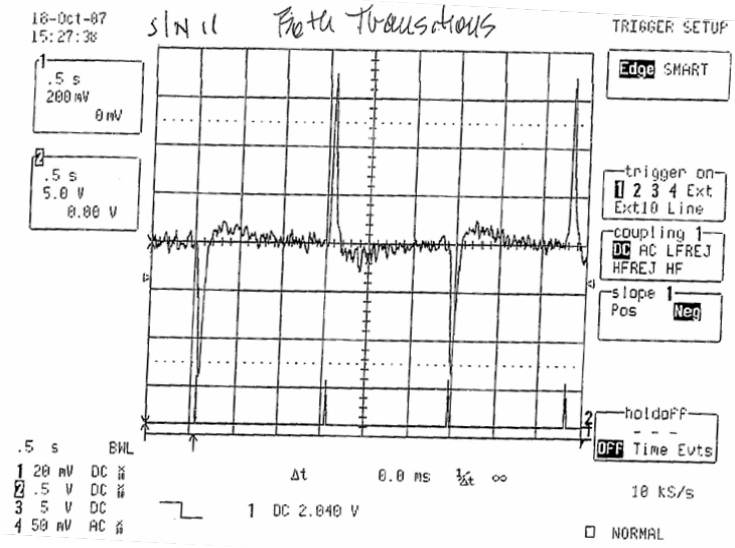

Figure 8.12: HCI performance sample collected by vendor during shutter wheel test.

to-sky or sky-to-Earth). That data is input into the Roll and Rate Determination block. Using the geometry shown in Figure 8.8, this data is converted into values for Ω, then using Eq. 8.1, a roll angle is determined. This procedure is performed over a range of known roll angles. The mean and standard deviation of the error of the reported angle

is shown in Figures 8.13 and 8.14.

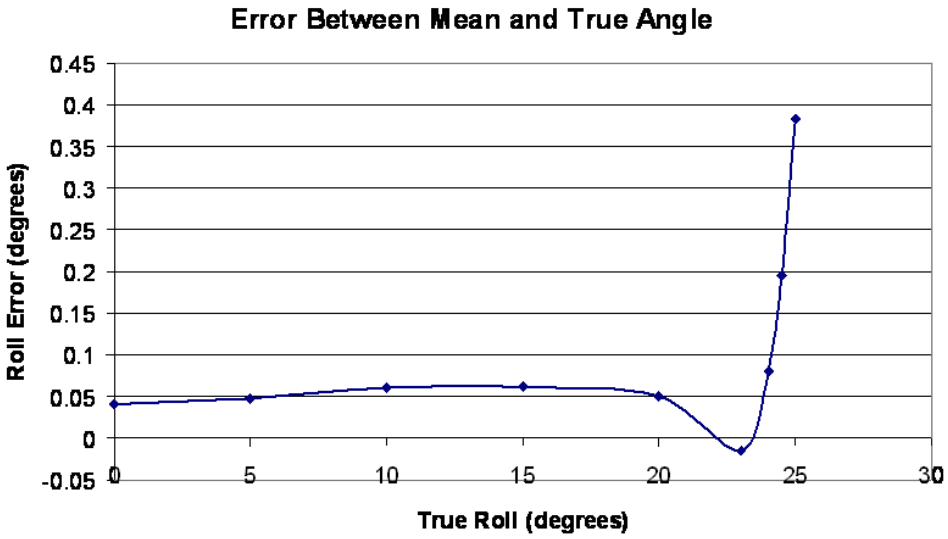

Figure 8.13: Roll determination error as a function of angle from horizontal.

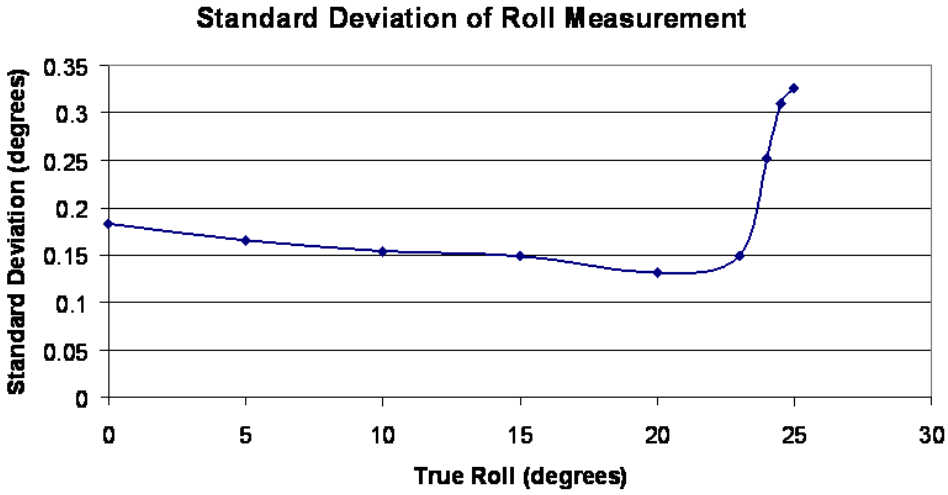

Figure 8.14: Roll determination standard deviation as a function of angle from horizontal.

Both the mean and the standard deviation of the roll error begin to grow sharply

at angles above 23°. That angle may be improved by optimizing the angle between the HCIs, but 23° serves as a conservative baseline. In the worst-case attitude configuration, this means that the spacecraft will have a true anomaly span of 46° of continuous good-crossing data. Data taken within 3° of the beginning and end of this span will satisfy the separation requirement of 4.ADC5.1 and 4.ADC5.2.

Sample roll data outputs of the Roll and Rate Determination block at two points in orbit are fed to the Spin Axis Determination block, which implements the intersection of two cones method to calculate a single spin vector in 3-space. A visualization of these results is shown in Figure 8.15.

The determination simulation is repeated with the same true initial conditions several thousand times to examine the effect that the sensor white noise has on the overall determination process. A histogram of this data appears in Figure 8.16.

The mean of the distribution in Figure 8.16 is 2.11° with a standard deviation of 2.14°. Roughly 50% of the time, the spin axis is determined to less than 1° of true.

As shown, this data does not satisfy the knowledge requirement of 2.ADC3. However, this data is generated with only two full rotations (four crossings) of data. The data can be expected to improve as $1/\sqrt{n}$, so with the ten crossings required by 4.ADC5.1, the mean error drops well below the 2° required in 2.ADC3. 4.ADC5.1 and 5.2 are therefore set to require ten consecutive crossings.

Beyond increasing the number of samples, there are other methods of improving the attitude determination scheme. Because there is such a distinct mode of results under 1° of error, a filtering scheme could be implemented to remove data from the bell-shaped second mode between 2° and 10°. Additionally, a filtering process at the roll determination level to removing crossings outside two standard deviations of the mean could also greatly improve the data.

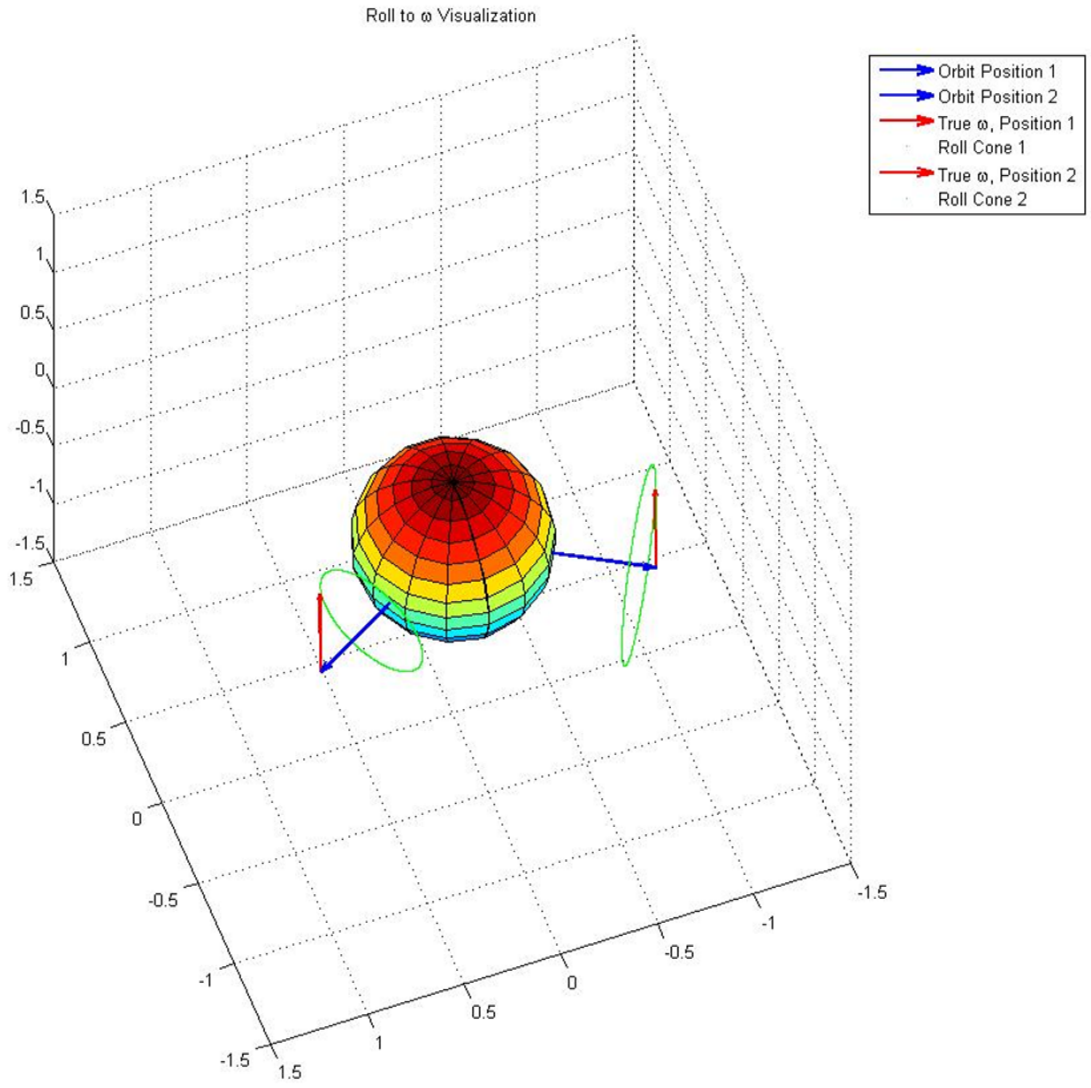

Figure 8.15: Visualization of two cones of ambiguity and their intersections within the simulation.

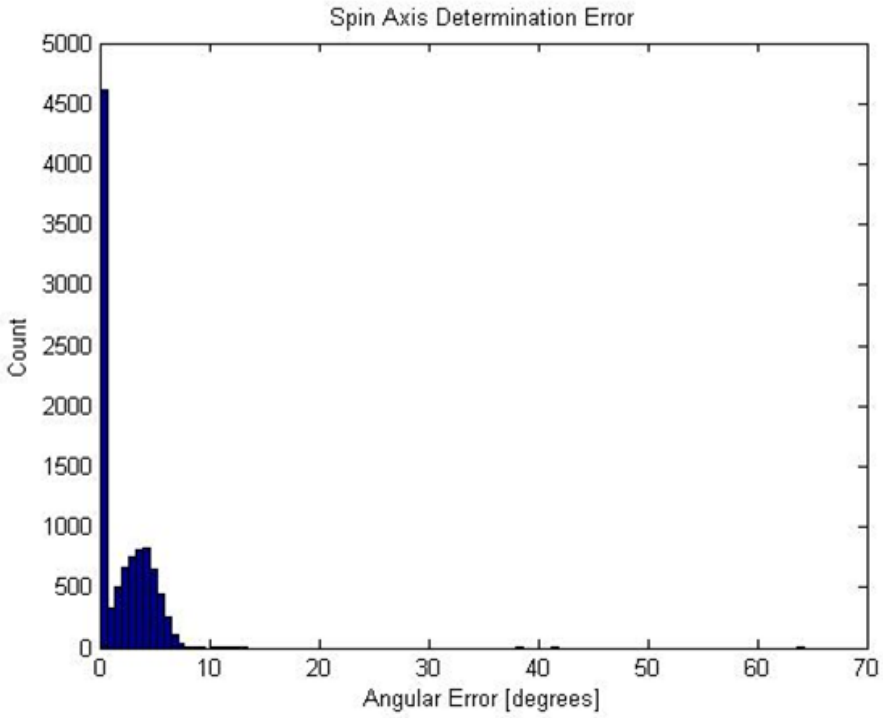

Figure 8.16: Angular error distribution generated by Monte Carlo simulation of HCIs and determination algorithm.

8.6 Conclusion

The baseline configuration of the Horizon Crossing Indicator and the two-cone intersection determination scheme has been shown to satisfy 2.ADC3 and all of its children requirements in a worst-case attitude configuration.

The performance of the determination system could be greatly improved with a number of simple modifications, including:

- Filtering out crossings outside two standard deviations from the mean interval time
- Optimizing the angle between the HCIs and the spin axis
- Implementing a batch processor algorithm to estimate the attitude state of the spacecraft based on statistical (rather than deterministic) methods

Chapter 9

Conclusion

An Attitude Determination and Control system for a micro-class student satellite is designed and analyzed.

The design process follows a systematic engineering approach. The process begins with a Requirements Flow Down document generated at the system level. Requirements are then flowed to the ADC subsystem. A trade study is performed against these requirements to determine the type of stabilization, method of control, and hardware suite best suited for the DANDE mission. The final architecture decision is a orbit-normal spinning spacecraft which spins-up autonomously, but performs spin axis alignment to orbit normal using an open-loop control scheme. Partial attitude determination is done with one three-axis magnetometer during spinup and two horizon crossing indicators during normal operations. Active control is achieved with two ferromagnetic core torque rods (one in the direction of the spin axis and one transverse to it) and a passive, fluid-filled ring nutation damper dissipates kinetic energy to pull the spacecraft into a pure spin about the major principal axis of inertia.

After architecture design choices are made, and individual components and algorithms are specified based on these requirements. To validate component and algorithm level requirements, numerical analysis is performed on both the control and determination aspects of the system. This analysis is verified with comparison to heritage missions.

To aid in requirements validation, an attitude simulation tool is developed in MATLAB. This tool is used to analyze the spinup maneuver and to evolve the control algorithm. This tool also plays a role in the worst-case attitude analysis described in this document.

Once the requirements are validated, the components are designed to these requirements. The torque rods and nutation damper, which are to be manufactured in house, are designed to performance parameters named by these requirements.

Much work remains to be done on the ADC subsystem. Algorithms must be optimized, both in the spinup and alignment maneuvers. The determination scheme stands to benefit greatly from implementing a filter on the data. On the hardware side, test procedures must be written and verified, and then the hardware must be integrated into the rest of the system.

Bibliography

[1] Andrew D. Anderson, Jerry J. Sellers, and Yoshi Hashida. Attitude determination and control system simulation and analysis for low-cost micro-satellites. In Aerospace Conference Proceedings, volume 5.6, pages 2935–2949. IEEE, 13 March 2004.

[2] Walter Benenson, John W. Harris, Horst Stocker, and Holger Lutz, editors. Handbook of Physics, page 443. Springer-Verlag, New York, 2002.

[3] P. G. Bhuta and L. R. Koval. A viscous ring damper for a freely precessing satellite. International Journal of Mechanical Science, 8:383–395, 1966.

[4] Timothy Holden. Snoe annular nutation damper design methodology. Technical report, Laboratory for Atmospheric and Space Physics, Jun 2005.

[5] Timothy Holden. Snoe instrument timing delay calculations. Technical report, Laboratory for Atmospheric and Space Physics, Jul 2005.

[6] J. A. Larsen, R. Amini, and R. Izadi-Zamanabadi. Advanced attitude control of pico sized satellites. IAC, 05:1–7, 2006.

[7] Wiley J. Larson and James R. Wertz, editors. Space Mission Analysis and Design. Microcosm Press, El Segundo, CA, third edition, 2004.

[8] Kenneth Moe and Mildred Moe. Method for deriving densities and in-track winds during storms. In Astrodynamics Specialist Conference and Exhibit, 6396. AIAA/AAS, 2006.

[9] Gregg Radtke. Magnetic torquer overview. Technical Report GNC-014, University of Arizona Student Satellite Project, Dec 1999.

[10] Fabio Santoni and Fabio Bolotti. Attitude determination of small spinning spacecraft using three axis magnetometer and solar panel data. In Aerospace Conference Proceedings, pages 129–133. IEEE, 2000.

[11] Hanspeter Schaub and John L. Junkins. Analytical Mechanics of Space Systems. American Institute of Aeronautics and Astronautics, Inc., Reston, Virginia, 2003.

[12] Asim K. Sen. A nutation damper for a dual-spin spacecraft. IEEE Transactions on Aerospace and Electronic Systems, AES-6(6):129–133, 1970.

[13] Stanley C. Solomon. The student nitric oxide explorer. In Space Sciencecraft Control and Tracking in the New Millennium, number 121 in 2810. Proc. SPIE, 1996.

[14] W. S. Stanley. Quaternion from rotation matrix. Journal of Guidance and Control, 1(3):223–224, 1978.

[15] Byron D. Tapley, Bob E. Schutz, and George H. Born. Statistical Orbit Determination. Elsevier Academic Press, Burlington, Massachusetts, 2004.

[16] B. E. Tossman. Variable paramter nutation damper for asa-a. Journal of Spacecraft, 8(7):743, Jul 1971.

[17] R. Weiss. Sensing accuracy of a conical scan co_2 horizon sensor. Journal of Spacecraft, 9(8):607–612, 1972.